IEEE Access
Multidisciplinary | Rapid Review | Open Access Journal

Received April 7, 2019, accepted April 27, 2019, date of publication May 7, 2019, date of current version May 21, 2019.

Digital Object Identifier 10.1109/ACCESS.2019.2915395

A Stochastically Geometrical Poisson Point Process Approach for the Future 5G D2D Enabled Cooperative Cellular Network

FAIZAN QAMAR[1], KAHARUDIN DIMYATI[1], MHD NOUR HINDIA[1], KAMARUL ARIFFIN NOORDIN[1], AND IRAJ SADEGH AMIRI[2,3]

[1]Department of Electrical Engineering, Faculty of Engineering, University of Malaya, Kuala Lumpur 50603, Malaysia
[2]Computational Optics Research Group, Advanced Institute of Materials Science, Ton Duc Thang University, Ho Chi Minh City 700000, Vietnam
[3]Faculty of Applied Sciences, Ton Duc Thang University, Ho Chi Minh City 700000, Vietnam

Corresponding author: Kaharudin Dimyati (kaharudin@um.edu.my)

This work was supported by the Engineering and Physical Sciences Research Council (EPSRC) under Grant EP/P028764/1 (UM IF035-2017).

ABSTRACT Due to recent developments in the cellular communication system, stochastic process implementation is necessary. The cellular communication system exhibits random patterns in various domains, thereby compelling the utilization of stochastic processes to achieve an optimal output. User behaviors with respect to the variable geographical pattern, population density, architecture, data usage, and mobility over various cells are random in nature. Therefore, the stochastic-geometry-based Poisson point process (PPP) technique can be implemented to accurately analyze these random processes in device-to-device (D2D)-based cooperative cellular networks. The stochastic modeling entails the consideration of transmitters and receivers as the elements of stochastic point processes. The hexagonal method is not applicable for the implementation of heterogeneous network topologies, as it is not suitable for topologies, in which the cell size is not fixed. Therefore, a randomly designed heterogeneous network uses stochastic geometry as a viable solution for predicting the probabilistic parameters, including the cell interference, load distribution, coverage probability, base station (BS) mapping, and signal-to-interference-plus-noise ratio (SINR). Moreover, as a network architecture that is based on relay nodes (RNs), cellular and D2D users can be utilized in the domain of homogeneous random models. The associated phenomenon can be considered independent and Poisson. In this paper, the stochastic-geometric-based PPP approach is introduced for modeling the SINR, success probability, ergodic capacity, and outage probability for the D2D-enabled cooperative cellular network. The proposed PPP realistic model utilizes BS, RN, the cellular user (CU), and D2D user positioning method to design an interference-free network. The success probability, ergodic capacity, and outage probability for cellular and D2D users are used as metrics for evaluating the results with respect to various SINR threshold values and node densities. Moreover, the total success probability, ergodic capacity, and outage probability have been calculated for various multiple-input-multiple-output (MIMO) antenna configurations to validate the results. The results confirmed that the proposed PPP model approach outperforms the grid model and conventional multi-antenna ultra-dense network (UDN) approaches.

INDEX TERMS 5G, stochastic geometry, interference cancellation, multi-hop communication, Poisson point process (PPP), D2D enabled cellular network.

I. INTRODUCTION

Due to the recent escalation in the utilization of communication devices, the pursuit of higher bandwidth has become imperative [1]. Several researchers, mobile operators, and the 3rd Generation Partnership Project (3GPP) are collaborating to achieve higher throughput with larger user capacity [2]. The next-generation mobile network will be referred to as the fifth generation (5G) network and is expected to be commercialized in the year 2020 [3], [4]. The expected data rate for the 5G network is approximately 100 Gbps with maximum latency of 1 ms, along with better user capacity and battery

The associate editor coordinating the review of this manuscript and approving it for publication was Xiaofan He.

life [5], [6]. In order to achieve an acceptable quality of service (QoS), various potential solutions are being developed, such as the use of the millimeter-wave (mm-wave) frequency band [7]–[9], massive MIMO [10], cooperative network using RNs [11], coordinated multi-point operation (CoMP) [12], wireless software-defined networking (WSDN) [13], D2D communication [14], internet of things (IoT) [15], [16], ethernet passive optical network (EPON) [17], and big data & mobile cloud computing [18]. The 5G network will be capable of incorporating existing technologies, such as several advanced power optimization techniques [19], [20] and optimal scheduling algorithms [21]. Furthermore, the 5G network will be designed to be compatible with various enabling technologies, such as network function virtualization (NFV), advanced radio access techniques, and green communication [22].

In a wireless urban area network, most users fall victim to excessive interference by nearby devices and suffer scattering issues. This phenomenon is due to the high user density, numerous buildings, and unpredictable obstacles [23], [24]. Therefore, users who are located on a cell edge experience weaker signals than the minimum desired signal level that is required for seamless connectivity [12]. In this scenario, deploying a small BS within the cell to boost the signal strength for the cell edge users is not considered a viable solution [25], [26] because it can increase the inter-cell interference, which would require more complex coordinated scheduling algorithms and incur high unnecessary costs [27]. In order to address this issue, a highly feasible solution is to deploy an infrastructure-based transceiver to establish a multiple-hop communication network [28], in which a transceiver acts as an RN to service mobile users with higher efficiency and low cost [29]. This solution is the key advancement and a recommended solution for 5G networks, especially for ultra-dense areas, to satisfy the increasing demand for diversity and coverage extensions [30], [31]. Multiple RNs can be deployed to achieve diversity improvement and higher user throughput by utilizing a better performing modulation and coding scheme (MCS) [32], [33]. Using the full-duplex topology in a cooperative network is the most efficient approach for providing maximum throughput at the destination; however, it also leads to various undesired inter- and intra-cell interferences, along with relay self-interference. Mitigation of these interferences is essential for achieving a higher received SINR.

According to recent investigations of D2D and cellular cooperative networks, the unlicensed spectrum of cellular networks can be shared by D2D users at the access level within the same network [34], [35]. Hence, D2D can be used to reduce the transmission overhead at the access network to improve the performance of the core network of the cellular system [36]. This network is commonly termed the D2D-enabled cooperative cellular network, which is illustrated in Figure 1. Setting up D2D wireless networks can be a smart approach for maximizing the scarce spectrum resources whereby the unlicensed spectrum is utilized via

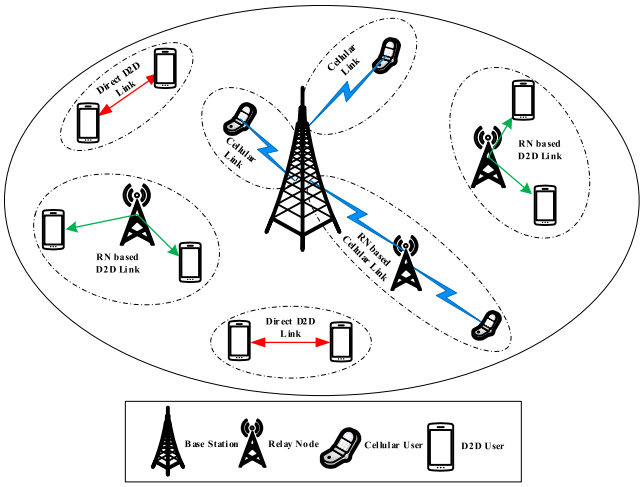

FIGURE 1. D2D-Enabled Cooperative Cellular Network.

coordinated radio resource (CRR) management [37], [38]. High inter-cell interference is often encountered between various D2D adjacent networks and between D2D and cellular networks, along with D2D network boundary ambiguity [39]. Likewise, the overall mobile network system capacity can be significantly improved by deploying a wide range of spectrum bands to serve individual D2D networks [40]. The D2D-enabled cooperative cellular network will play a key role in the upcoming 5G network in terms of improved latency, spectrum efficiency, and power efficiency, as well as network capacity enlargement, and network coverage extension [41]–[43].

Recent advances in cellular communication systems have confirmed the importance of stochastic geometry and its applications. The behavior of the cellular and D2D users in a random geographic area that spans over different cells can be analyzed better with PPP, thereby making it the most convenient approach in the current emerging technology. Stochastic modeling considers the network of transmitters and receivers as the realization of stochastic point processes [44], [45]. The homogenous random model can be utilized in this type of architecture, and the processes can be considered independent and Poisson. Each process has convenient mathematical properties [46]; hence, this model is frequently defined in Euclidean space and used as a mathematical model for seemingly random processes. This model utilizes the Poisson distribution, for which the intensity measure is the mean density of points [47]. The simplicity of the Poisson process makes it easier to implement in the relay network scenario [48], [49]. While designing realistic models, e.g., 2D realizations of BSs on a square or hexagonal lattice, various parameters, including the positions of the RNs, CUs, and D2D users and cell-edge users, along with their received SINRs, must be considered. Moreover, a model must be deeply scanned, provided that an interference-limited environment is available where the BSs are deployed, namely, an environment in which no external noise is created by the interference of the

RNs, CUs, and D2D users [50]. Since the channel conditions are not static and can cause random changes in terms of the shadowing and fading effects, the variation in the received SINR, which causes impulsive user throughput, is a crucial issue to be mitigated. The most common constraints that cause such changes are i) the user density in the specified area, ii) the height of the transmitting antenna, and iii) the radius of the cell. These parameters strongly affect the performance of heterogeneous and relay networks that are deployed in urban and suburban regions [51]. Overall enhanced network performance with superior SINR and throughput can be achieved by improving the network architecture where the BSs, RNs, and cellular and D2D users are deployed through stochastic modeling [52].

II. CONTRIBUTIONS

Network planning and design are the most important steps in network geometry modeling that increase in complexity when a D2D-enabled cooperative cellular network is considered. Various unconventional methods can be employed to address complicated scenarios to create a realistic scheme. Enabling a D2D network in a cellular network facilitates the exploitation of the direct communication between the CUs, thereby improving the spectrum utilization, energy efficiency and overall throughput of the network. However, the users in a multi-hop D2D-enabled cooperative cellular network suffer from various interferences such as intra and inter-cell interferences that can be from nearby cells, RNs, CUs, or D2D users, which affects the user SINR and can cause the ambiguous received signal. This study investigates additional interference issues that arise while enabling the D2D network in the existing cellular network. A new PPP approach has been formulated that encompasses a wide variety of interferences by considering a multi-hop high-density D2D-enabled cooperative cellular network in which the signal is transferred from BS-to-D2D by crossing three network hops: the BS-to-RN, RN-to-CU, and CU-to-D2D. A stochastic geometric-based PPP approach is utilized to model the SINR and success probability for D2D-enabled cooperative cellular networks. Then, low complex spatial interference cancellation is applied to model the success probability, average capacity, and outage probability for the individual network hops. The performance of the proposed PPP model approach has been compared with those of the grid model and conventional multi-antenna UDN approaches. Subsequently, the results have been evaluated in terms of the success probability, ergodic capacity and outage probability for cellular and D2D users at various SINR thresholds and cell densities. Moreover, to verify the proposed PPP model, the total success probability, ergodic capacity and outage probability from BS-to-D2D have been calculated under various MIMO antenna configurations.

The remainder of the paper is organized as follows: Section 3 reviews the recent literature on interference in D2D-enabled cellular networks and highlights the limitations of the available approaches. Section 4 presents the network system model. Section 5 discusses the calculation of SINR for user hops from the BS-to-RN, RN-to-CU, and CU-to-D2D. In addition, mathematical models for the success probability before and after the interference cancellation effect, the ergodic capacity, and the outage probability are presented in this section. Section 6 presents the results of the comparison of the proposed PPP model with the grid model and the conventional multi-antenna UDN model, and Section 7 presents the conclusions of this study.

III. LITERATURE REVIEW

The D2D-enabled cooperative cellular network has several advantages; however, various technical challenges are encountered, e.g., in device discovery, node finding, and interference management. The future-generation wireless systems, such as the 5G network and beyond, are expected to implement efficient interference management mechanisms to achieve more reliable communication [53]. With the advent of D2D technology, users can now communicate over multiple interfaces in the same shared access network. The fundamental challenge in the D2D-enabled cooperative cellular network is to mitigate the unwanted signal during cellular and D2D transmissions, which can coexist within the same frequency channel. One method for achieving this goal is to reduce the transmission power of users within the confinement of the D2D region of the network, rather than reducing the transmission power of the cellular systems, which tends to create an imbalance between the downlink and uplink coverage. However, this method will affect the overall network performance. Several studies have recently been conducted on concerning mitigation of the interference effect in the D2D-enabled cooperative cellular network, a few of which are discussed below.

The stochastic-geometry-based PPP model is one of the efficient models for mitigating interference in the network and helps to improve the overall system performance. The authors in [54] have investigated the signal-to-interference ratio (SIR) meta-distribution depending on the wireless node location. These authors have used the PPP approach to model BSs and D2D users using the meta-distribution and have calculated the mean local delay to analyze the analytical expression. The proposed techniques have been demonstrated to be beneficial for D2D receivers and downlink CUs, while maintaining the probabilities of cellular and D2D users, even if the user density varies. Moreover, in [55], the authors have focused on the estimation of the data session blocking probability to increase the energy efficiency and characterize the energy expenditure for D2D users. These authors have proposed licensed and unlicensed bands for modeling the D2D system using PPP for users' formulations. The results confirm that their methodology accurately models the interworking cooperation between 3GPP LTE and Wi-Fi-Direct technologies with a significant achieved gain. Another approach, which is presented in [56], focuses on the performance of the cellular and D2D underlay uplink cellular network. The authors have used the fractional frequency reuse (FFR) technique to minimize the interference between

cellular and D2D users. According to the results, by modeling the spatial distribution of D2D users as a homogeneous PPP, the overall system coverage has been improved. In another approach, the interference characterization of the D2D underlay network, along with the consideration of spatial and social relationships, has been investigated [57]. The authors have performed spatial and social distributions of interfering D2D nodes and have utilized the Zipf-based marked PPP approach to achieve a thinned independently marked PPP (IMPPP) process. This method has simplified the power control and enhanced the physical distance that satisfies the capacity demands. In [58], massive MIMO energy efficiency with the power beacon (PB) technique has been investigated. The PPP hybrid network, with the consequent positions of cellular and D2D users, helps boost the sufficient probability of D2D communications.

Moreover, the authors in [59] have focused on the performance analysis network model of D2D, along with RF energy harvesting. These authors have utilized a PPP stochastic geometric model for the BS distribution, in combination with the Ginibre determinantal point process (DPP). This approach is used to investigate the combination of the peer-to-peer simultaneous wireless information and power transfer (SWIPT) strategy and RF transmitters. The results are compared with those of the PPP approach for the downlink multichannel cellular network. The proposed method performs better under the D2D condition in combination with SWIPT transmission and energy harvesting. Another approach has been studied for the coverage enhancement of cellular networks. This approach utilizes the stochastic geometry-based PPP approach and the Laplace function to decrease the path loss and determine the shortest pair distance [60]. The analytical criterion-based D2D pairing is excluded in this methodology. The proposed method has outperformed the conventional method in terms of the coverage probability of CUs. Moreover, the authors in [61] have studied a distance-based power control scheme for uplink cellular networks. These authors have proposed a stochastic geometry-based PPP model for analyzing the coverage performance of both CUs and D2D users. In their study, these authors have succeeded in increasing the system performance by reusing cellular frequency resources. The authors in [62] have investigated D2D user allocation with multiband heterogeneous networks. This study utilized a stochastic geometry system model that is based on the Lagrange function and the Karush–Kuhn–Tucker (KKT) conditions. The results confirmed that the proposed approach successfully mitigates interferences and increases the D2D transmission capacity. In [63], the mixed joint mode transmission pair for cellular and D2D networks has been studied. The authors proposed an analytical model that is based on stochastic geometry and focused on i) cellular/D2D mode selection in which the nearest BS receives the power and ii) a D2D pairing scheme that focuses on the nth-nearest neighbor as the serving node for the receiver interest. The results show that the proposed method significantly increases the system sum throughput and widens the coverage probability. The authors in [64] have focused on the performance of UDN for multi-antenna receivers. The proposed approach adopted the stochastic-geometry-based framework for integral expressions and tight tractable approximations for the probability of successful transmission. This approach assumes that no more than half of the available degrees of freedom should be used for interference cancellation. The results demonstrated the efficiency of the proposed model compared with other conventional techniques.

Furthermore, in a practical wireless system, the network traffic varies both spatially and temporally, which may substantially affect the performance of the network. Several studies have been conducted to examine this phenomenon, such as [65], in which the authors proposed a new approach that is based on the combination of stochastic geometry and queuing theory for the design of ultra-dense traffic fluctuating networks. Various spatiotemporal arrival properties of traffic fluctuations are discussed, along with promising solutions such as dynamic time-vision duplexing and a full-duplex radio. Similarly, an approach reported in [66] also utilizes the combination of a stochastic geometry tool with queuing theory to evaluate the tradeoff between the end-to-end delay and the physical-layer security for wireless networks. The approach involves splitting the message into two separate packets and analyzing the effect on the mean delay and the secrecy outage probability. The results confirmed that the proposed approach delivers superior results for backlogged and dynamic scenarios, even if the number of transmitters is large. Another approach was proposed in [67] for mitigating interferences, in which a tractable analytical model for large-scale heterogeneous IoT networks was designed. This approach utilizes a Poisson cluster process (PCP) approach, which takes the correlations among the device locations into account. This approach is highly suitable for the distribution process of devices, especially for low-power wide-area (LPWA) IoT-based networks. The results demonstrated higher QoS performance with an optimal energy operation control policy for IoT devices.

The state-of-the-art related work is summarized in Table 1.

IV. SYSTEM MODEL

In this model, we have considered a D2D-enabled multi-tier cellular network that consists of 3-tiers: i) a BS that is connected to an RN (BS-to-RN), ii) an RN that is connected to CUs (RN-to-CU), and iii) a CU that is connected to a D2D user (CU-to-D2D). This network is illustrated in Figure 2. The complete D2D-enabled cooperative cellular network, along with the received (useful and interference) signals, is illustrated in Figure 3. The RNs, CUs and D2D users are distributed randomly based on the stochastic geometry with the PPPs of ψ_R, ψ_{CU}, and ψ_D, respectively. The transmission power constraints for the BSs, RNs, CUs, and D2D users are defined as $\rho_{BS}\left\{|x_{BS}|^2\right\} = 1$, $\rho_R\left\{|x_R|^2\right\} = 1$, $\rho_{CU}\left\{|y_{CU}|^2\right\} = 1$, and $\rho_D\left\{|z_D|^2\right\} = 1$, respectively. The densities of the RNs, CUs and D2D users

TABLE 1. Summary of the related work.

Scenarios/Issues	Methodologies	Advantages	Limitations/Future Work	References
SIR calculation using a meta-distribution depends on the wireless node location	BS modeling for the meta-distribution and the mean local delay analytical expression calculations have been performed	D2D receivers and downlink CU moments unchanged, if $\lambda_C(P_C / P_D)^{\sigma}$ remains constant	Limited to fixed user location	[54]
Estimation of data session blocking probability to raise mobile devices energy efficiency and expenditure characterization	Licensed and unlicensed band for D2D system model has been designed using PPP for entire users' formulations	Significant increase in network capacity	Capacity performance can be further improved by further reducing interference	[55]
Minimizing the interference between D2D and CU underlay uplink cellular network	Fractional frequency reuse (FFR) methodology has been used to reduce interference	Increase in system capacity while reducing the user's interference	Focused on only uplink cellular network underlay	[56]
Interference characterization of D2D underlay users	Utilization of the Zipf-based marked PPP approach to achieve IMPPP	Simplified power control with higher achieved capacity	Limited to a single cell network	[57]
D2D massive MIMO energy efficiency with power beacons (PBs)	PPP hybrid network with consequent position of CUs, D2D users and PBs	Boost sufficient probability of D2D communication	Relay self-interference effect is not included in the scenario	[58]
Performance analysis of the D2D network model along with the RF energy harvesting model	BS distribution with PPP stochastic geometry models in combination with the Ginibre Determinantal point process (DPP)	DPP distribution provides works better with SWIPT transmission and energy harvesting compared to the PPP approach	Power splitter receiver increases the cost of the system	[59]
Coverage enhancement in the cellular network	PPP approach with cooperation of the Laplace functional to decrease path loss and obtain the shortest pair distance	Better coverage probability of the cellular user compared with the conventional approach	Cell radius limited to a 500 m distance	[60]
The distance-based power control scheme for the uplink cellular network	Stochastic geometry-based PPP approach to analyze the coverage performance of both cellular and D2D users	Boost system performance by reusing cellular frequency resources	Focused on the uplink cellular network underlay	[61]
D2D user allocation scheme with multi-bands for the heterogeneous networks	Stochastic geometry system model based on the Lagrange function and KKT conditions	Achieved better results compared with the average distributing method	Palm probability of the Poisson process effect is not considered	[62]
Joint mode with the pair mixed cellular and D2D network	Analytical model with stochastic geometry focused on i) cellular/D2D mode selection ii) D2D pairing scheme	Increases system sum throughput along with better coverage probability	Self-interference effect is practically impossible to completely cancel	[63]
Performance analysis of UDNs for the multi-antenna receivers for the probability of successful transmission	Stochastic geometry-based framework for integral expressions and tight tractable approximations	Theoretical theory stating that no more than half of the available degrees of freedom should be used for interference cancellation	Limited to uplink transmission only	[64]
Traffic matching in 5G UDN	An approach based on the combination of stochastic geometry and queuing theory for the design of ultra-dense traffic fluctuating network	Various spatiotemporal arrival properties of traffic fluctuation are highlighted	More complicated practical scenarios with different types of traffic need to be explored	[65]
Tradeoff between delay and physical layer security in wireless networks	The approach involves splitting the message into two sperate packets and analyzing the effect on mean delay and secrecy outage probability	Delivers better results for backlogged as well as dynamic scenarios even when the number of transmitters is increased	Encoding and decoding of the message signal increase complexity	[66]
Mitigation of interferences in which a tractable analytical model for large-scale heterogeneous IoT network is designed.	Utilization of a Poisson cluster process (PCP) approach, which takes the correlation among the device location	Better QoS performance with optimal energy operation control policy for IoT devices, especially for the low power wide-area (LPWA) IoT-based network	The coverage factor needs to be investigated with an improved communication distance	[67]

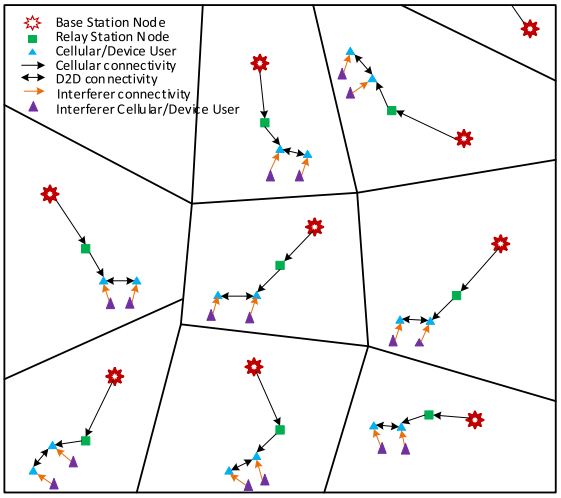

FIGURE 2. Network Scenario.

are denoted as λ_R, λ_{CU}, andλ_D, respectively. We assume that all channels in our network, namely, $\|H_{BS_iR_i}\|$, $\|H_{R_jR_i}\|$, $\|H_{R_iR_i}\|$, $\|H_{R_iCU_i}\|$, $\|H_{R_jCU_i}\|$, $\|H_{CU_jCU_i}\|$, $\|H_{D_jCU_i}\|$, $\|H_{CU_iD_i}\|$, $\|H_{R_iD_i}\|$, $\|H_{CU_jD_i}\|$, and $\|H_{D_jD_i}\|$, are experiencing Rayleigh fading $\sigma \succ \exp(\sigma)$, with path-loss exponent α with its coefficient γ.

The fading factors for RNs, CUs, and D2D users are expressed as $h \succ \exp(1), f \succ \exp(1)$, and $g \succ \exp(1)$, respectively. Moreover, the intensities of the RNs, CUs, and D2D users are denoted as Υ_R, Υ_{CU}, and Υ_D. The RNs are operated in full-duplex mode, where the reception and transmission of signals occur simultaneously on the same frequency band. The decode-and-forward protocol is utilized, in which the message signal from the BS is decoded and subsequently re-encoded prior to transmission to the CUs. In our network, we assume that each RN is connected to a single BS and all other signals from other BSs are considered the interference signal. Similarly, each CU is served by the nearest RN, and all other signals at the RN are considered the interference signal; D2D users are served by the nearest CU, and all signals from other sources are considered the interference signal. The entries of each matrix are independent and identically distributed (i.i.d.) and follow a complex Gaussian distribution with zero mean and variance Ω^2. In a random-access network, the user must be located at the origin to examine the network performance. The results will be obtained using the Palm probabilities of Poisson processes, which will not affect the process statistics due to the stationary position of the receiver in PPP. Table 2 shows all the nomenclature that would be used in the mathematical model presented in the next section.

V. CHANNEL MODEL

As shown in Figure 3, in the first tier (BS-to-RN) of our network model, the RN, namely, R_i, receives various signals, such as the desired signal (DS) x_{BS_i} from BS_i via channel

TABLE 2. Nomenclature.

Symbol	Definition
x_{BS}	Transmit signal from BS
x_R	Transmit signal from RNs
x_{CU}	Transmit signal from CU Nodes
x_D	Transmit signal from D2D User
y_R	Received signal at RNs
y_{CU}	Received signal at CUs
y_D	Received signal at D2D Users
ρ_{BS}	Transmission power at BS
ρ_R	Transmission power at RN
ρ_{CU}	Transmission power at CUs
ρ_D	Transmission power at D2D Users
$\|H_{BS\,R}\| or \|H_{R\,BS}\|$	Channel between BS and RN
$\|H_{R\,CU}\| or \|H_{CU\,R}\|$	Channel between RN and CU
$\|H_{CU\,CU}\|$	Channel between CU and CU
$\|H_{R\,R}\|$	Channel between RN and RN
$\|H_{CU\,D}\| or \|H_{D\,CU}\|$	Channel between D2D user and CU
$\|H_{D\,D}\|$	Channel between D2D and D2D user
$P_{L,RR}$	Path loss of IRI having $\|H_{RR}\|$
$P_{L,M}$	Path loss of DS having $\|H_{BSR}\|$
$P_{L,O}$	Path loss of RUI having $\|H_{RCU}\|$
$P_{L,P}$	Path loss of CCI having $\|H_{CUCU}\|$
$P_{L,Q}$	Path loss of RDI having $\|H_{RD}\|$
$P_{L,N}$	Path loss of CDI or DDS having $\|H_{CUD}\| or \|H_{DCU}\|$
$P_{L,R}$	Path loss of DDI having $\|H_{DD}\|$
γ	Path loss exponent
f	Fading factor (Rayleigh distribution for RNs)
g	Fading factor (Rayleigh distribution for CUs)
h	Fading factor (Rayleigh distribution for D2D Users)
$I_{T_{CU}}$	Total interference of CUs
I_R	Interference from RNs
I_{CU}	Interference from CUs
I_D	Interference from D2D Users
N_{D2D}	Number of received antenna at D2D user
λ_R	RNs density
λ_{CU}	CUs density
λ_D	D2D users density
$P_{SUC_{R_i}}$	Probability of successful transmission at RNs
$P_{SUC_{CU_i}}$	Probability of successful transmission at CUs
$P_{SUC_{D_i}}$	Probability of successful transmission at D2D Users
$P_{SUC(K)_{R_i}}$	Probability of successful transmission at RNs after interference calculation
$P_{SUC(K)_{CU_i}}$	Probability of successful transmission at CUs after interference calculation
$P_{SUC(K)_{D_i}}$	Probability of successful transmission at D2D Users after interference calculation
$P_{OUT_{R_i}}$	Outage probability at RN
$P_{OUT_{CU_i}}$	Outage probability at CU
$P_{OUT_{D_i}}$	Outage probability at D2D User
P_{OUT_T}	Total outage probability
ς_{BS-RN}	Capacity for BS-to-RN
ς_{RN-CU}	Capacity for RN-to-CU
ς_{CU-D2D}	Capacity for CU-to-RN
ς_T	Total ergodic capacity of the Network

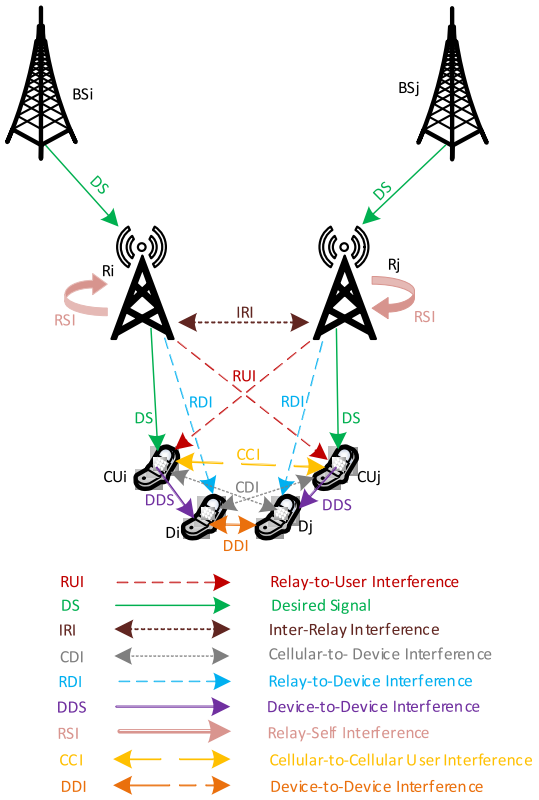

FIGURE 3. Network Model.

$\|H_{BS_iR_i}\|$ with path loss $P_{L,M}$, and multiple undesired signals y_{R_i}, such as the inter-relay interference (IRI) from R_j by signal x_{R_j} via channel $\|H_{R_jR_i}\|$ with path loss $P_{L,RR}$, the relay-self interference (RSI) via channel $\|H_{R_iR_i}\|$ and the received noise n_{R_i} from the transmission channel. Similarly, for the second tier (RN-to-CU), the CU_i receives signal y_{CU_i}, which consists of DS x_{R_i} from R_i via channel $\|H_{R_iCU_i}\|$ with path loss $P_{L,O}$, the relay-to-user interference (RUI) from R_j with signal x_{R_j} via channel $\|H_{R_jCU_i}\|$ with path loss $P_{L,O}$, the cellular-to-cellular interference (CCI) from CU_j with signal x_{CU_j}via channel $\|H_{CU_jCU_i}\|$ with path loss $P_{L,P}$, the cellular-to-device interference (CDI) from D_j with signal x_{D_j} via channel $\|H_{D_jCU_i}\|$ with path loss $P_{L,N}$, and the received noise n_{CU_i} from the channel. Similarly, for the third tier (CU-to- D2D), D_i receives signals y_{D_i} from multiple sources, such as the DDS with signal x_{CU_i} from CU_i via channel $\|H_{CU_iD_i}\|$ with path loss $P_{L,N}$, the relay-to-device interference (RDI) with signal x_{R_i} from R_i via channel $\|H_{R_iD_i}\|$ with path loss $P_{L,Q}$, the cellular-to-device interference (CDI) from CU_j with signal x_{CU_j}via channel $\|H_{CU_jD_i}\|$ with path loss $P_{L,N}$, the device-to-device interference (DDI) from D_j with signal x_{D_j} via channel $\|H_{D_jD_i}\|$ with path loss $P_{L,R}$, and the transmission noise n_{D_i} from the channel.

A. SINR CALCULATION

As illustrated in Figure 3, the CU link consists of three hops: the BS-to-RN, RN-to-CU, and CU-to-D2D. Here we determine the SINR between BS-to-RN in the first link.

1) BS-TO-RN HOP

Building on Slivnyak's theorem [68], [69], consider a BS, namely, BS_i, which is located at the origin. Due to the stationarity of ϕ_{BS_i}, we express the statistics of the received signal at RN R_i. The received signal y_{R_i} at R_i is the sum of DS plus all interferences from nearby sources.

$$y_{R_i} = \sqrt{\rho_{BS_i}}\, P_{L,M}\alpha^{-\frac{\gamma}{2}} \|H_{BS_iR_i}\| x_{BS_i} + n_{R_i} + \sqrt{\rho_{R_i}} \|H_{R_iR_i}\| x_{R_i} + \sum_{x_{Rj}\in\psi_R} \sqrt{\rho_{R_j}}\, P_{L,RR}\alpha^{-\frac{\gamma}{2}} \|H_{R_jR_i}\| x_{R_j} \quad (1)$$

where the first term represents the DS from BS_i plus the noise that is received at R_i, the second term represents the RSI, and the third term represents the IRI from the neighboring RN R_j. In the RSI, the RN transmitter and receiver have the same stationary position; therefore, no channel path loss is considered.

Suppose the received signal is specified. The SINR at R_i is expressed as follows:

$$SINR_{R_i} = \frac{\rho_{BS_i} P_{L,M}\alpha_i^{-\gamma} \|H_{BS_iR_i}\|^2}{I_{R_i} + n_{R_i}} \quad (2)$$

where I_{R_i} is the overall interference at R_i, i.e., RSI and IRI.

$$I_{R_i} = \sqrt{\rho_{R_i}} \|H_{R_iR_i}\| x_{R_i} + \sum_{x_{Rj}\in\psi_R} \sqrt{\rho_{R_j}}\, P_{L,RR}\alpha^{-\frac{\gamma}{2}} \|H_{R_jR_i}\| x_{R_j} \quad (3)$$

In our network, the transmission power at the RNs, namely, ρ_R, is much lower than the transmission power at the BS, namely, ρ_{BS}. The RNs lie in their corresponding BS cells, which are separated by a non-zero distance; therefore, in this case, the IRI can be neglected. Moreover, we assume an interference-limited environment; therefore, the noise n_{R_i} is much smaller than all the interferences, i.e., $n_{R_i} \ll I_{R_i}$. Thus, the noise effect is negligible in this scenario.

2) RN-TO-CU HOP

For the second hop, namely, from the RN-to-CU, the received signal at CU_i consists of DS from R_i plus the received noise and all the interferences: RUI from R_j, CCI from CU_j and CDI from D_j.

$$y_{CU_i} = \sqrt{\rho_{R_i}}\, P_{L,O}h^{-\frac{\gamma}{2}} \|H_{R_iCU_i}\| x_{R_i} + n_{CU_i} + \sum_{x_{Rj}\in\psi_R} \sqrt{\rho_{R_j}}\, P_{L,O}h^{-\frac{\gamma}{2}} \|H_{R_jCU_i}\| x_{R_j} + \sum_{x_{CU_j}\in\psi_{CU}} \sqrt{\rho_{CU_j}}\, P_{L,P}f^{-\frac{\gamma}{2}} \|H_{CU_jCU_i}\| x_{CU_j} + \sum_{x_{Dj}\in\psi_D} \sqrt{\rho_{D_j}}\, P_{L,N}g^{-\frac{\gamma}{2}} \|H_{D_jCU_i}\| x_{D_j} \quad (4)$$

Suppose the received signal is specified. The SINR at CU_i is expressed as follows:

$$SINR_{CU_i} = \frac{\rho_{R_i} P_{L,O}h_i^{-\gamma} \|H_{R_iCU_i}\|^2}{I_{CU_i} + n_{CU_i}} \quad (5)$$

where I_{CU_i} is the overall interference at CU_i , i.e., RUI, CCI, and CDI.

$$I_{CU_i} = \sum_{x_{Rj}\in\psi_R} \sqrt{\rho_{R_j}}\, P_{L,O} h^{-\frac{\gamma}{2}} \left\| H_{R_j CU_i} \right\| x_{R_j} + \sum_{x_{CU_j}\in\psi_{CU}} \sqrt{\rho_{CU_j}}\, P_{L,P} f^{-\frac{\gamma}{2}} \left\| H_{CU_j CU_i} \right\| x_{CU_j} + \sum_{x_{Dj}\in\psi_D} \sqrt{\rho_{D_j}}\, P_{L,N} g^{-\frac{\gamma}{2}} \left\| H_{D_j CU_i} \right\| x_{D_j} \quad (6)$$

Here, also we assume an interference-limited environment; therefore, the noise n_{CU_i} is much smaller than all the interferences, i.e., $n_{CU_i} \ll I_{CU_i}$. Thus, the noise effect is negligible in this scenario.

3) CU-TO-D2D HOP

For the third hop, namely, from CU-to-D2D, the received signal at D_i is the combination of DS from CU_i plus the received noise, with interferences such as RDI from R_i, CDI from CU_j, and DDI from D_j.

$$y_{D_i} = \sqrt{\rho_{CU_i}}\, P_{L,N} f^{-\frac{\gamma}{2}} \left\| H_{CU_i D_i} \right\| x_{CU_i} + n_{D_i} + \sum_{x_{Rj}\in\psi_R} \sqrt{\rho_{R_i}}\, P_{L,Q} h^{-\frac{\gamma}{2}} \left\| H_{R_i D_i} \right\| x_{R_i} + \sum_{x_{CU_j}\in\psi_{CU}} \sqrt{\rho_{CU_j}}\, P_{L,N} f^{-\frac{\gamma}{2}} \left\| H_{CU_j D_i} \right\| x_{CU_j} + \sum_{x_{D_j}\in\psi_D} \sqrt{\rho_{D_j}}\, P_{L,R} g^{-\frac{\gamma}{2}} \left\| H_{D_j D_i} \right\| x_{D_j} \quad (7)$$

Suppose the received signal is specified. The SINR at D_i is expressed as follows:

$$SINR_{D_i} = \frac{\rho_{CU_i}\, P_{L,N} f_i^{-\gamma} \left\| H_{CU_i D_i} \right\|^2}{I_{D_i} + n_{D_i}} \quad (8)$$

where I_{D_i} is the overall interference at D_i, i.e., RDI, CDI, and DDI.

$$I_{D_i} = \sum_{x_{Rj}\in\psi_R} \sqrt{\rho_{R_i}}\, P_{L,Q} h^{-\frac{\gamma}{2}} \left\| H_{R_i D_i} \right\| x_{R_i} + \sum_{x_{CU_j}\in\psi_{CU}} \sqrt{\rho_{CU_j}}\, P_{L,N} f^{-\frac{\gamma}{2}} \left\| H_{CU_j D_i} \right\| x_{CU_j} + \sum_{x_{D_j}\in\psi_D} \sqrt{\rho_{D_j}}\, P_{L,R} g^{-\frac{\gamma}{2}} \left\| H_{D_j D_i} \right\| x_{D_j} \quad (9)$$

Here, also we assume an interference-limited environment; therefore, the noise n_{D_i} is much smaller than all the interferences, i.e., $n_{D_i} \ll I_{D_i}$. Thus, the noise effect is negligible in this scenario.

The success probability for all individual hops, namely, BS-to-CU, RN-to-CU, and CU-to-D2D, will be calculated in the next section.

B. SUCCESS PROBABILITY

The successful probabilities for full transmission (BS-to-D2D) are given by a joint complementary cumulative distribution function (CCDF) of $SINR_{R_1}$, $SINR_{CU_i}$, and $SINR_{D_i}$ and denoted by $P_{SUC_{R_i}}$, $P_{SUC_{CU_i}}$ and $P_{SUC_{D_i}}$, respectively [70]. Due to the independent sampling of the point process, there is no correlation between these hops and the total success probability is the scalar product of $P_{SUC_{R_i}} P_{SUC_{CU_i}}$, and $P_{SUC_{D_i}}$.

$$P_{SUC_T} = P_{SUC_{R_i}} \cdot P_{SUC_{CU_i}} \cdot P_{SUC_{D_i}} \quad (10)$$

According to Fortuin-Kasteleyn-Ginibre inequality [71], the system performance for the uncorrelated case can be considered as a lower bound. The success probabilities for the three individual hops are calculated below.

1) BS-TO-RN HOP

In this section, we analyze the success probability of the BS-to-RN hop. It is defined as the probability that the obtained SINR at RN R_i (as estimated in equation 2) exceeds a predefined threshold, denoted as τ_R, and can be expressed as

$$P_{SUC_{R_i}} \cong P\left(SINR_{R_i} \geq \tau_R\right) \quad (11)$$

which is the CCDF of the $SINR_{R_i}$; here, τ_R is the minimum SINR threshold for detecting the transmitted messages successfully. This threshold satisfies a targeted SINR, and the probability of success at R_i is

$$P_{SUC_{R_i}} \cong P\left(\frac{\rho_{BS_i} P_{L,M} \alpha_i^{-\gamma} \left\| H_{BS_i R_i} \right\|^2}{I_{R_i}} \geq \tau_R\right) \quad (12)$$

$$P_{SUC_{R_i}} \cong P\left(\left\| H_{BS_i R_i} \right\|^2 \geq \tau_R \rho_{BS_i}^{-1} P_{L,M}^{-1} \alpha_i^{\gamma} I_{R_i}\right) \quad (13)$$

$$P_{SUC_{R_i}} \cong \int_0^{\infty} P\left(\left\| H_{BS_i R_i} \right\|^2 \geq \tau_R \rho_{BS_i}^{-1} P_{L,M}^{-1} \alpha_i^{\gamma} s\right) \cdot f_{I_{R_i}}(s) ds \quad (14)$$

$$P_{SUC_{R_i}} \cong \int_0^{\infty} F_{R_i}^{c}\left(\tau_R \rho_{BS_i}^{-1} P_{L,M}^{-1} \alpha_i^{\gamma} s\right) \cdot f_{I_{R_i}}(s) ds \quad (15)$$

where equation 15 is obtained by conditioning S and its CCDF denoted by $F_{R_i}^{c}$.

Theorem 1: Let the interfering relays' transmitters form a Poisson process of intensity Υ_R around RN R_i receivers. The success probability of the BS-to-RN hop is calculated as

$$P_{SUC_{R_i}} \cong \sum_{i=0}^{N_{Ri}-1} \left[\frac{(-s)^i}{i!} \frac{d^i}{ds^i} \xi_{I_{R_i}}(s)\right]_{s=\tau_R \rho_{BS_i}^{-1} P_{L,M}^{-1} \alpha_i^{\gamma}} \quad (16)$$

where $\xi_{I_{R_i}}(s)$

$$\xi_{I_{R_i}}(s) \cong \frac{1}{\left(1 + s\rho_{BS_i}\right)^{\gamma}} e^{(-\lambda_R \alpha(s))} \quad (17)$$

is the Laplace transform of the interference I_{R_i}, as explained in Theorem 1 of [72] and where we have defined

$$\alpha(s) \cong \int_0^{\infty} \left(2\pi - \frac{1}{1 + s\rho_{BS_i} P_{L,M} \alpha_i^{-\gamma}} \vartheta(s, f)\right) \cdot f df \quad (18)$$

with

$$\vartheta\,(s,f) \cong \frac{1}{2\pi}\int_0^{2\pi} \times \frac{\breve{d}\varphi}{1+s\rho_{BS_i}\left(\breve{d}_{BS-RN}+f^2+2\breve{d}_{BS-RN}f\cos\varphi\right)^{-\frac{\gamma}{2}}} \quad (19)$$

Here, $\breve{d}_{BS-RN}$ represents the minimum distance between the BS-to-RN. Note that all terms in the summation are positive since the n^{th} derivative of $\xi_{\mathrm{I}_{R_i}}$ is negative for odd n.

Proof: Refer to Appendix A.

According to Theorem 1, the employment of multiple receive antennas results in an array, and the larger the value of N_{R_i}, the more terms are summed to obtain $P_{SUC_{R_i}}$, as expressed in equation 16. All the summed terms are positive since the n^{th} derivative of $\xi_{\mathrm{I}_{R_i}}(s)$ is negative for all odd n.

The result in Theorem 1 provides a fundamental limit on the BS-to-RN hop, and its performance in an interference-limited scenario. It has a looser integral form $\alpha\,(s)$ for the success probability $P_{SUC_{R_i}}$, which is not in closed form and must be evaluated numerically; however, tight lower and upper bounds can be obtained in Corollary 1 as follows.

Corollary 1: From equation 16, the Laplace transform of I_{R_i} is bounded as

$$\xi_{\mathrm{I}_{R_i}}(s) \in \left[\xi^{\min}_{\mathrm{I}_{R_i}}(s), \xi^{\max}_{\mathrm{I}_{R_i}}(s)\right] \quad \text{(i)}$$

where

$$\xi^{\min}_{\mathrm{I}_{R_i}}(s) \cong \frac{1}{\left(1+s\rho_{BS_i}\right)^{\gamma}} e^{\left(-\lambda_R \alpha^{\max}(s)\right)} \quad \text{(ii)}$$

$$\xi^{\max}_{\mathrm{I}_{R_i}}(s) \cong \frac{1}{\left(1+s\rho_{BS_i}\right)^{\gamma}} e^{\left(-\lambda_R \alpha^{\min}(s)\right)} \quad \text{(iii)}$$

where we have defined

$$\alpha^{\max}\,(s) \cong 2\left(\rho_{BS_i}+\rho_{R_i}\right)\frac{\pi^2 s^{\frac{2}{\gamma}}}{\gamma\sin\left(\frac{2\pi}{\gamma}\right)} \quad \text{(iv)}$$

$$\alpha^{\min}\,(s) \cong \left(1+\frac{2}{\gamma}\right)\left(\rho_{BS_i}+\rho_{R_i}\right)\frac{\pi^2 s^{\frac{2}{\gamma}}}{\gamma\sin\left(\frac{2\pi}{\gamma}\right)} \quad \text{(v)}$$

To obtain the success probability of the BS-to-RN hop $P_{SUCR_i}(\tau_R)$, which is equal to $P_{SUC_{R_i}}(\tau_R)^{\max} \cdot P_{SUC_{R_i}}(\tau_R)^{\min}$, substitute the upper and lower bounds $\xi_{\mathrm{I}_{R_i}}(s) \in [\xi^{\min}_{\mathrm{I}_{R_i}}(s), \xi^{\max}_{\mathrm{I}_{R_i}}(s)]$ are substituted in $P_{SUC_{SR_i}}$, as shown in equation 16.

Proof: Refer to Appendix B.

Next, the success probability analysis for the RN-to-CU hop is calculated.

2) RN-TO-CU HOP

In this section, we analyze the success probability of the RN-to-CU hop, which is defined as the probability that the obtained SINR at CU_i (as estimated in equation 5) exceeds a predefined threshold τ_{CU} and can be expressed as

$$P_{SUC_{CU_i}} \cong P\left(SINR_{CU_i} \geq \tau_{CU}\right) \quad (20)$$

which is the CCDF of the $SINR_{R_i}$; here, τ_{CU} is the minimum SINR threshold for detecting the transmitted messages successfully. This threshold satisfies a targeted SINR and the probability of success at CU_i is

$$P_{SUC_{CU_i}} \cong P\left(\frac{\rho_{R_i}\mathrm{P}_{L,O}h_i^{-\gamma}\left\|H_{R_iCU_i}\right\|^2}{\mathrm{I}_{CU_i}} \geq \tau_{CU}\right) \quad (21)$$

$$P_{SUC_{CU_i}} \cong P\left(\left\|H_{R_iCU_i}\right\|^2 \geq \tau_{CU}\rho_{R_i}^{-1}\mathrm{P}_{L,O}{}^{-1}h_i^{\gamma}\mathrm{I}_{CU_i}\right) \quad (22)$$

$$P_{SUC_{CU_i}} \cong \int_0^{\infty} P\left(\left\|H_{R_iCU_i}\right\|^2 \geq \tau_{CU}\rho_{R_i}^{-1}\mathrm{P}_{L,O}{}^{-1}h_i^{\gamma}\mathrm{s}\right) \cdot f_{\mathrm{I}_{CU_i}}(s)ds \quad (23)$$

$$P_{SUC_{CU_i}} \cong \int_0^{\infty} F_{CU_i}{}^{c}\left(\tau_{CU}\rho_{R_i}^{-1}\mathrm{P}_{L,O}{}^{-1}h_i^{\gamma}\mathrm{s}\right) \cdot f_{\mathrm{I}_{CU_i}}(s)ds \quad (24)$$

where equation 24 is obtained by conditioning S, and the CCDF is denoted by $F^c_{CU_i}$.

As shown in Theorem 1 discussed in BS-to-RN hop, here the success probability for the RN-to-CU hop is calculated as

$$P_{SUC_{CU_i}} \cong \sum_{i=0}^{N_{CU_i}-1}\left[\frac{(-s)^i}{i!}\frac{d^i}{ds^i}\xi_{\mathrm{I}_{CU_i}}(s)\right]_{s=\tau_{CU}\rho_{R_i}^{-1}\mathrm{P}_{L,O}^{-1}h_i^{\gamma}} \quad (25)$$

where $\xi_{\mathrm{I}_{CU_i}}$ is the Laplace transform of the interference I_{CU_i} and can be estimated as explained in Theorem 1 of [72] and expressed as

$$\xi_{\mathrm{I}_{CU_i}}(s) \cong \frac{1}{\left(1+s\rho_{R_i}\right)^{\gamma}} e^{\left(-\lambda_{CU}\alpha(s)\right)} \quad (26)$$

This phenomenon explains how the employment of multiple receiver antennas results in an array: the larger the number of antennas N_{CU_i}, the more terms are summed to obtain $P_{SUC_{CU_i}}$, as expressed in equation 25.

According to Theorem 1 of [72], we can express

$$\alpha\,(s) \cong \int_0^{\infty} 2\pi\left(1-\frac{1}{1+s\rho_{R_i}\mathrm{P}_{L,O}\alpha_i^{-\gamma}}\vartheta\,(s,f)\right)\cdot g dg \quad (27)$$

with

$$\vartheta\,(s,g) \cong \frac{1}{2\pi}\int_0^{2\pi} \times \frac{d\varphi}{1+s\rho_{R_i}\left(\breve{\mathrm{d}}_{RN-CU}+g^2+2\breve{\mathrm{d}}_{RN-CU}g\cos\varphi\right)^{-\frac{\gamma}{2}}} \quad (28)$$

Here, $\breve{\mathrm{d}}_{RN-CU}$ represents the minimum distance between the RN-to-CU. Note that all terms in the summation are positive since the n^{th} derivative of $\xi_{\mathrm{I}_{CU_i}}$ is negative for odd n.

Proof: Refer to Appendix C.

The result in equation 25 provides a fundamental limit on the RN-to-CU hop and its performance in an interference-limited scenario. It has a looser integral form $\alpha(s)$ on the success probability $P_{SUC_{CU_i}}$, which is not in closed form and must be evaluated numerically; however, tight lower and upper bounds can be obtained from Corollary 1.

The bounds on the success probability of the RN-to-CU hop $P_{SUC_{CU_i}}(\tau_{CU})$, which are denoted by $P_{SUC_{CU_i}}(\tau_{CU})^{\max}$ and $P_{SUC_{CU_i}}(\tau_{CU})^{\min}$, can be calculated by substituting the upper and lower bounds $\xi_{\mathrm{I}_{CU_i}}(s) \in \left[\xi^{\min}_{\mathrm{I}_{CU_i}}(s), \xi^{\max}_{\mathrm{I}_{CU_i}}(s)\right]$ into the expression for $P_{SUC_{CU_i}}$, as shown in equation 25.

Next, the success probability for the CU-to-D2D hop is calculated.

3) CU-TO-D2D HOP

In this section, we analyze the success probability of the CU-to-D2D hop, which is defined as the probability that the obtained SINR at D2D user D_i (as estimated in equation 8) exceeds a predefined threshold τ_D and can be expressed as

$$P_{SUC_{D_i}} \cong P\left(SINR_{D_i} \geq \tau_D\right) \tag{29}$$

which is the CCDF of $SINR_{D_i}$; here, τ_D is the minimum SINR threshold for detecting the transmitted messages successfully, namely, the specified threshold should satisfy a target SINR. The probability of success at the destination is

$$P_{SUC_{D_i}} \cong P\left(\frac{\rho_{CU_i}\,\mathrm{P}_{L,N} f_i^{-\gamma}\,\left\|H_{CU_iD_i}\right\|^2}{\mathrm{I}_{D_i}} \geq \tau_D\right) \tag{30}$$

$$P_{SUC_{D_i}} \cong P\left(\left\|H_{CU_iD_i}\right\|^2 \geq \tau_D \rho^{-1}_{CU_i}\,\mathrm{P}^{-1}_{L,N} f_i^{\gamma}\,\mathrm{I}_{D_i}\right) \tag{31}$$

$$P_{SUC_{D_i}} \cong \int_0^{\infty} P\left(\left\|H_{CU_iD_i}\right\|^2 \geq \tau_D \rho^{-1}_{CU_i}\,\mathrm{P}^{-1}_{L,N} f_i^{\gamma}\right) \cdot f_{\mathrm{I}_{D_i}}(s)ds \tag{32}$$

$$P_{SUC_{D_i}} \cong \int_0^{\infty} F^{c}_{D_i}\left(\tau_D \rho^{-1}_{CU_i}\,\mathrm{P}^{-1}_{L,N} f_i^{\gamma} s\right) \cdot f_{\mathrm{I}_{D_i}}(s)ds \tag{33}$$

where equation 33 is obtained by conditioning S, and the CCDF is denoted by $F^{c}_{D_i}$.

Similar to Theorem 1, in which the BS-to-RN hop was considered, the success probability analysis for the CU-to-D2D hop is calculated as

$$P_{SUC_{D_i}} \cong \sum_{i=0}^{N_{D_i}-1} \left[\frac{(-s)^i}{i!}\frac{d^i}{ds^i}\xi_{\mathrm{I}_{D_i}}(s)\right]_{s=\tau_D \rho^{-1}_{CU_i}\,\mathrm{P}^{-1}_{L,N} f_i^{\gamma}} \tag{34}$$

where $\xi_{\mathrm{I}_{D_i}}$ is the Laplace transform of the interference I_{D_i}, estimated as explained in Theorem 1 of [72] and expressed as

$$\xi_{\mathrm{I}_{D_i}}(s) \cong \frac{1}{\left(1+s\rho_{CU_i}\right)^{\gamma}} e^{(-\lambda_D \alpha(s))} \tag{35}$$

This finding explains how the employment of multiple receiver antennas results in an array: the larger the number of antennas N_{D_i}, the more terms are summed to obtain $P_{SUC_{D_i}}$, as expressed in equation 34.

According to Theorem 1 of [72], we define

$$\alpha(s) \cong \int_0^{\infty}\left(2\pi - \frac{1}{1+s\rho_{CU_i}\,\mathrm{P}_{L,N} f_i^{-\gamma}}\vartheta(s,f)\right)\cdot hdh \tag{36}$$

with

$$\vartheta(s,h) \cong \frac{1}{2\pi}\int_0^{2\pi} \times \frac{d\varphi}{1+s\rho_{CU_i}\left(\check{\mathrm{d}}_{CU-D2D}+h^2+2\check{\mathrm{d}}_{CU-D2D}h\cos\varphi\right)^{-\frac{\gamma}{2}}} \tag{37}$$

Here, $\check{\mathrm{d}}_{CU-D2D}$ represents the minimum distance between the CU-to-D2D. Note that all terms in the summation are positive since the n^{th} derivative of $\xi_{\mathrm{I}_{D_i}}$ is negative for odd n.

Here, we can recall the distances between BS-to-RN and RN-to-CU and CU-to-D2D hop, given the definition of $\vartheta(s,T)$

$$\vartheta(s,T) \in [\vartheta(s,f), \vartheta(s,g), \vartheta(s,h)] \tag{38}$$

$$\vartheta(s,T) \in \left[\frac{1}{1+s\rho_{BS}\left(\check{\mathrm{d}}_{BS-RN}\right)^{-\gamma}}, \frac{1}{1+s\rho_{R}\left(\check{\mathrm{d}}_{RN-CU}\right)^{-\gamma}}, \frac{1}{1+s\rho_{CU}\left(\check{\mathrm{d}}_{CU-D2D}\right)^{-\gamma}}\right] \tag{39}$$

The result in equation 34 provides a fundamental limit on the CU-to-D2D hop and its performance in an interference-limited scenario. It has a looser integral form $\alpha(s)$ for the success probability $P_{SUC_{D_i}}$, which is not in closed form and must be evaluated numerically; however, tight lower and upper bounds can be obtained from Corollary 1.

The success probabilities of the CU-to-D2D hop $P_{SUC_{D_i}}(\tau_D)$, which are denoted by $P_{SUC_{D_i}}(\tau_D)^{\max}$ and $P_{SUC_{D_i}}(\tau_D)^{\min}$, can be calculated by substituting upper and lower bounds $\xi_{\mathrm{I}_{D_i}}(s) \in \left[\xi^{\min}_{\mathrm{I}_{D_i}}(s), \xi^{\max}_{\mathrm{I}_{D_i}}(s)\right]$ into the expression for $P_{SUC_{CU_i}}$ from Corollary 1.

C. INTERFERENCE CANCELLATION

In this section, we have applied interference cancellation at the three receiving nodes: R_i,CU_i and D_i. Low complex spatial interference cancellation, which is also known as partial zero forcing (PZF), has been applied [64], [73]. The three hops, namely, BS-to-RN, RN-to-CU and CU-to-D2D, are subjected to K_i interference cancellations, where $K_{R_i} \leq N_{R_i}-1$, $K_{CU_i} \leq N_{CU_i}-1$and $K_{D_i} \leq N_{D_i}-1$, respectively, in which the remaining degree of freedom are utilized to increase the received signal quality.

1) BS-TO-RN HOP

To achieve a higher receiving SINR at RN R_i, undesired interferences, such as the interference from nearby RNs and the relay self-interference, must be mitigated. In an interface-limited scenario, the cancellation of interferences is very

essential. Let us express the points of $\Phi_{RN} \in (i,j)$ in increasing order at RN: $\{R_j \in R_{j+1}\}_{j=1}^{\infty}$. The low complex spatial partial zero-forcing (PFZ) interference cancellation is applied to cancel K_{R_i} interferences at R_i. Here, Φ_{RN} represents the coverage area of RN, which includes (i,j). Let's recall the overall interference at R_i, namely, I_{R_i}, which is defined in equation 3.

$$\mathrm{I}_{R_i(K)} = \sqrt{\rho_{R_i}} \left\| H_{R_i R_i} \right\| x_{R_i} + \sum_{x_{Rj} \in \psi_R} \sqrt{\rho_{R_j}}\, \mathrm{P}_{L,RR} \alpha^{-\frac{\gamma}{2}} \left\| H_{R_j R_i} \right\| x_{R_j} \tag{40}$$

where $\mathrm{I}_{R_i(K)}$ is the interference need to mitigate. The success probability of the BS-to-RN hop with PFZ can be stated as

$$P_{SUC(K)_{R_i}} \cong \sum_{i=0}^{K_{R_i}-N_{Ri}-1} \left[\frac{(-s)^i}{i!} \frac{d^i}{ds^i} \xi_{\mathrm{I}_{R_i(K)}}(s) \right]_{s=\tau_R \rho_{BS_i}^{-1} \mathrm{P}_{L,M}^{-1} \alpha_i^{\gamma}} \tag{41}$$

where $\xi_{\mathrm{I}_{R_i(K)}}(s)$ is the Laplace transform of $\mathrm{I}_{R_i(K)}$

$$\xi_{\mathrm{I}_{R_i(K)}}(s) \cong \frac{1}{1 + s\rho_{BS_i} \mathrm{P}_{L,M} \alpha_i^{-\gamma}} \times \left[\bigcup_{\substack{j \in \Phi_{RN} \\ j \le K_{R_i}}} \frac{1}{1 + s\rho_{BS_i} \mathrm{P}_{L,M} \alpha_i^{-\gamma}} \right] \tag{42}$$

Proof: Refer to Appendix D.

2) RN-TO-CU HOP

Similarly, to achieve a higher receiving SINR at the CU, undesired interferences, such as the interferences from nearby RNs, CUs and D2D users, must be mitigated. Let us sort the points of $\Phi_{CU} \in (i,j)$ in increasing order at CU, namely, $\{CU_j \in CU_{j+1}\}_{j=1}^{\infty}$, and apply PFZ to cancel K_{CU_i} interferences at CU_i. Here, Φ_{CU} represents the coverage area of CU, which includes (i,j). Let us recall the overall interference at CU_i, namely, I_{CU_i}, which is defined in equation 6.

$$\begin{aligned} \mathrm{I}_{CU_i(K)} = & \sum_{x_{Rj} \in \psi_R} \sqrt{\rho_{R_j}}\, \mathrm{P}_{L,O} h^{-\frac{\gamma}{2}} \left\| H_{R_j CU_i} \right\| x_{R_j} \\ & + \sum_{x_{CU_j} \in \psi_{CU}} \sqrt{\rho_{CU_j}}\, \mathrm{P}_{L,P} f^{-\frac{\gamma}{2}} \left\| H_{CU_j CU_i} \right\| x_{CU_j} \\ & + \sum_{x_{Dj} \in \psi_D} \sqrt{\rho_{D_j}}\, \mathrm{P}_{L,N} g^{-\frac{\gamma}{2}} \left\| H_{D_j CU_i} \right\| x_{D_j} \end{aligned} \tag{43}$$

where $\mathrm{I}_{CU_i(K)}$ is the interference needed to mitigate. The success probability of the RN-to-CU hop with PFZ can be stated as

$$P_{SUC(K)_{CU_i}} \cong \sum_{i=0}^{K_{CU_i}-N_{CU_i}-1} \times \left[\frac{(-s)^i}{i!} \frac{d^i}{ds^i} \xi_{\mathrm{I}_{CU_i(K)}}(s) \right]_{s=\tau_{CU} \rho_{R_i}^{-1} \mathrm{P}_{L,O}^{-1} h_i^{\gamma}} \tag{44}$$

where $\xi_{\mathrm{I}_{CU_i(K)}}(s)$ is the Laplace transform of the $\mathrm{I}_{CU_i(K)}$

$$\xi_{\mathrm{I}_{CU_i(K)}}(s) \cong \frac{1}{1 + s\rho_{R_i} \mathrm{P}_{L,O} \alpha_i^{-\gamma}} \times \left[\bigcup_{\substack{j \in \Phi_{RN} \\ j \in \Phi_{CU} \\ j \in \Phi_{D2D} \\ j \le K_{CU_i}}} \frac{1}{1 + s\rho_{R_i} \mathrm{P}_{L,O} \alpha_i^{-\gamma}} \right] \tag{45}$$

Proof: Refer to Appendix D.

3) CU-TO-D2D HOP

Likewise, to achieve a higher receiving SINR at the D2D user, undesired interferences, such as interferences from nearby RNs, CUs and D2D users, must be mitigated. In an interface-limited scenario, the canceling of interferences is essential. Let us express the points of $\Phi_{D2D} \in (i,j)$ in increasing order at the D2D user, namely, $\{D_j \in D_{j+1}\}_{j=1}^{\infty}$, and the PFZ is applied to cancel K_{D2D_i} interferences at D_i. Here, Φ_{D2D}represents the coverage area of the D2D user, which includes (i,j). Let us recall the overall interference at D_i, namely, I_{D_i}, which is defined in equation 9.

$$\begin{aligned} \mathrm{I}_{D_i(K)} = & \sum_{x_{Rj} \in \psi_R} \sqrt{\rho_{R_i}}\, \mathrm{P}_{L,Q} h^{-\frac{\gamma}{2}} \left\| H_{R_i D_i} \right\| x_{R_i} \\ & + \sum_{x_{CU_j} \in \psi_{CU}} \sqrt{\rho_{CU_j}}\, \mathrm{P}_{L,N} f^{-\frac{\gamma}{2}} \left\| H_{CU_j D_i} \right\| x_{CU_j} \\ & + \sum_{x_{D_j} \in \psi_D} \sqrt{\rho_{D_j}}\, \mathrm{P}_{L,R} g^{-\frac{\gamma}{2}} \left\| H_{D_j D_i} \right\| x_{D_j} \end{aligned} \tag{46}$$

where $\mathrm{I}_{D_i(K)}$ is the interference needed to mitigate. The success probability of the CU-to-D2D hop with PFZ can be stated as

$$P_{SUC(K)_{D_i}} \cong \sum_{i=0}^{K_{D_i}-N_{D_i}-1} \times \left[\frac{(-s)^i}{i!} \frac{d^i}{ds^i} \xi_{\mathrm{I}_{D_i(K)}}(s) \right]_{s=\tau_D \rho_{CU_i}^{-1} \mathrm{P}_{L,N}^{-1} f_i^{\gamma}} \tag{47}$$

where $\xi_{\mathrm{I}_{D_i(K)}}(s)$ is the Laplace transform of $\mathrm{I}_{D_i(K)}$

$$\xi_{\mathrm{I}_{D_i(K)}}(s) \cong \frac{1}{1 + s\rho_{CU_i} \mathrm{P}_{L,N} f_i^{-\gamma}} \times \left[\bigcup_{\substack{j \in \Phi_{RN} \\ j \in \Phi_{CU} \\ j \in \Phi_{D2D} \\ j \le K_{D2D_i}}} \frac{1}{1 + s\rho_{CU_i} \mathrm{P}_{L,N} f_i^{-\gamma}} \right] \tag{48}$$

Proof: Refer to Appendix D.

In the next section, the outage probability of R_i, CU_i and D_i are expressed.

D. OUTAGE PROBABILITY

The probability that $SINR_{R_i}$ falls below a given threshold level τ_R, is known as outage probability. For the first BS-to-RN hop, the following equations give the outage probability at R_i represented as $P_{OUT(K)_{R_i}}(\tau_R)$, which is the CCDF of $1 - SINR_{R_i}$ denoted as

$$P_{OUT(K)_{R_i}}(\tau_R) \cong P\left(SINR_{R_i} \leq \tau_R\right) \tag{49}$$

given by $P_{OUT(K)_{R_i}}(\tau_R) \cong 1 - e^{(-2\pi\Upsilon_R)}$ and stated as

$$P_{OUT(K)_{R_i}}(\tau_R) \cong 1 - P_{SUC(K)_{R_i}} \tag{50}$$

where $P_{SUC(K)_{R_i}}$ has been calculated in equation 41.

Similarly, for the RN-to-CU hop, where signals are received at CU_i, the probability that the $SINR_{CU_i}$ falls below a set threshold level of τ_{CU} is represented as $P_{OUT(K)_{CU_i}}(\tau_{CU})$, which is the CCDF of $1 - SINR_{CU_i}$ and expressed as

$$P_{OUT(K)_{CU_i}}(\tau_{CU}) \cong P\left(SINR_{CU_i} \leq \tau_{CU}\right) \tag{51}$$

given by $P_{OUT(K)_{CU_i}}(\tau_{CU}) \cong 1 - e^{(-2\pi\Upsilon_{CU})}$ and stated as

$$P_{OUT(K)_{CU_i}}(\tau_{CU}) \cong 1 - P_{SUC(K)_{CU_i}} \tag{52}$$

where $P_{SUC(K)_{CU_i}}$ has been calculated in equation 44.

Additionally, for the CU-to-D2D hop, the probability that $SINR_{D_i}$ at D_i falls below a set threshold level τ_D represented as $P_{OUT(K)_{D_i}}(\tau_D)$, which is the CCDF of $1 - SINR_{D_i}$ can be expressed as

$$P_{OUT(K)_{D_i}}(\tau_D) \cong P\left(SINR_{D_i} \leq \tau_D\right) \tag{53}$$

given by $P_{OUT(K)_{D_i}}(\tau_D) \cong 1 - e^{(-2\pi\Upsilon_D)}$ and stated as

$$P_{OUT(K)_{D_i}}(\tau_D) \cong 1 - P_{SUC(K)_{D_i}} \tag{54}$$

where $P_{SUC(K)_{D_i}}$ has been calculated in equation 47.

After determining the individual outage probability of each hop, the overall total outage probability denoted as $P_{OUT(K)_T}$ can be estimated as the scalar product of the individual probabilities as

$$P_{OUT(K)_T}(\tau) = P_{OUT(K)_{R_i}}(\tau_R) \cdot P_{OUT(K)_{CU_i}}(\tau_{CU}) \cdot P_{OUT(K)_{D_i}}(\tau_D) \tag{55}$$

In the next section, the ergodic capacity calculation for all individual hops are shown.

E. ERGODIC CAPACITY

Ergodic capacity is defined as the maximum rate of received signal that a user can achieve at the receiving end. The Shannon–Hartley theorem has been used to compute the ergodic capacity and calculated in bits/second. First, ergodic capacity for BS-to-RN hop (denoted as ς_{BS-RN}) can be determine as

$$\varsigma_{BS-RN} = \prod_{i=1}^{N_R} P_{SUC(K)_{R_i}} \log\left(1 + \tau_R\right) \tag{56}$$

where τ_R is minimum threshold SINR value at R_i and $P_{SUC(K)_{R_i}}$ is shown in equation 41.

Similarly, the ergodic capacity for the RN-to-CU hop (denoted as ς_{RN-CU}) can be calculated as

$$\varsigma_{RN-CU} = \prod_{i=1}^{N_{CU}} P_{SUC(K)_{CU_i}} \log\left(1 + \tau_{CU}\right) \tag{57}$$

where τ_{CU} is minimum threshold SINR value at CU_i and $P_{SUC(K)_{CU_i}}$ is defined in equation 44.

Likewise, the ergodic capacity for the CU-to-D2D hop (denoted as ς_{CU-D2D}) can be estimated as

$$\varsigma_{CU-D2D} = \prod_{i=1}^{N_{D2D}} P_{SUC(K)_{D_i}} \log\left(1 + \tau_D\right) \tag{58}$$

where τ_D is minimum threshold SINR value at D_i, and $P_{SUC(K)_{D_i}}$ is shown in equation 47.

After calculating the individual ergodic capacity or each hop, the overall total ergodic capacity denoted as ς_T can be estimated as the scalar product of the individual capacities

$$\varsigma_T = \varsigma_{BS-RN} \cdot \varsigma_{RN-CU} \cdot \varsigma_{CU-D2D} \tag{59}$$

VI. RESULTS AND DISCUSSION

In this section, the numerical results are presented to corroborate the proposed theoretical model. The results show that the proposed PPP model is robust to interference in the D2D-enabled cooperative cellular network. The results have been evaluated in terms of the success probability, ergodic probability and outage probability for cellular and D2D users at various SINR thresholds and node densities. Moreover, the success probability, ergodic capacity, and outage probability results have been evaluated for various MIMO antenna configurations. The performance of the proposed PPP model approach has been compared with those of the grid model and conventional multi-antenna UDN approaches [52], [74]. Monte Carlo simulations are utilized to evaluate the proposed scheme and averages are calculated over 1000 independent channel realizations. Table 3 lists the simulation parameters and their corresponding values.

According to the homogeneous PPP ψ_R in the Euclidean plane, the network model consists of BSs that are connected to RNs with an intensity Υ_R to serve cellular users. The intensity of each CU Υ_{CU} or D2D user Υ_D is assumed to be associated with the closest RNs in the Voronoi cell of the BSs, thereby resulting in coverage areas that comprise a Voronoi tessellation on the plane [75]. Two independent Poisson processes, namely, CU_i and D_i, represent the cellular and D2D users, respectively. Figure 4 illustrates the proposed PPP cellular model, where CUs are connected to their respective RNs and D2D users are connected to the nearby CUs to create a D2D network in the corresponding Voronoi cells. The cell structure has been designed according to the SINR value; the source has been deployed such that the users can achieve higher SINR values. Furthermore, a square lattice grid model for BSs, RNs, and cellular and D2D users with

TABLE 3. Simulation parameters.

Parameters	Values
Operating frequency	38 GHz
Number of Users	200
Number of RNs	25
Network Scenario	Urban (Random user deployment)
Cell size	20 km^2
Number of Transmit Antenna	2
Number of Receive Antenna	2, [2:8]
Path loss exponent (α)	3.8
Simulation Iteration	1000
SNR Threshold	~30db
RN transmission power	20 dBm
UE height	1 m
Antenna height	25 m
Number of RNs in a cell	1
Cell Radius	800 m

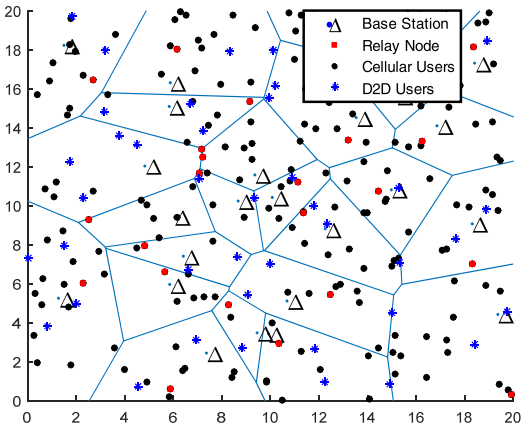

FIGURE 4. Network Deployment for the PPP Model.

eight interfering cells is shown in Figure 5. The deployment of multi-antenna UDN users is shown in Figure 6, where the cell has been designed according to the density of cellular and D2D users.

The SINR threshold represents a quantity that is used to limit the theoretical upper bound of the channel capacity in a network. This threshold defines the minimum signal for detecting the original transmitted signal. In the network under consideration, for the RN-to-CU hop, the signal that is transmitted from R_i and received at CU_i is referred to as the information signal, whereas any undesired signal at CU_i is considered an interfering signal. The relationships between the SINR threshold and the success probabilities prior to interference cancellation ($P_{SUC_{CU_i}}$) and after interference cancellation ($P_{SUC(K)_{CU_i}}$) are expressed in equation 25 and equation 44, respectively. The results regarding the success probability with respect to the SINR threshold at

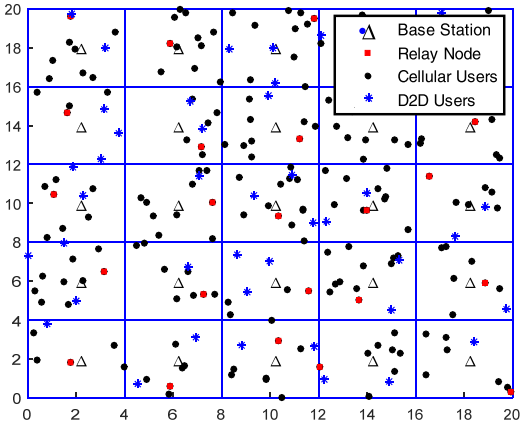

FIGURE 5. Network Deployment for the Square Grid Model.

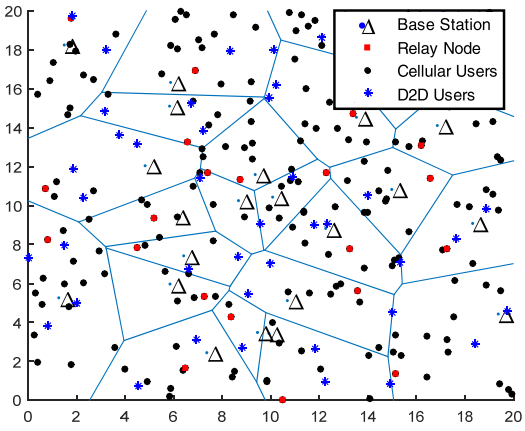

FIGURE 6. Network Deployment for the Multi-Antenna UDN Model.

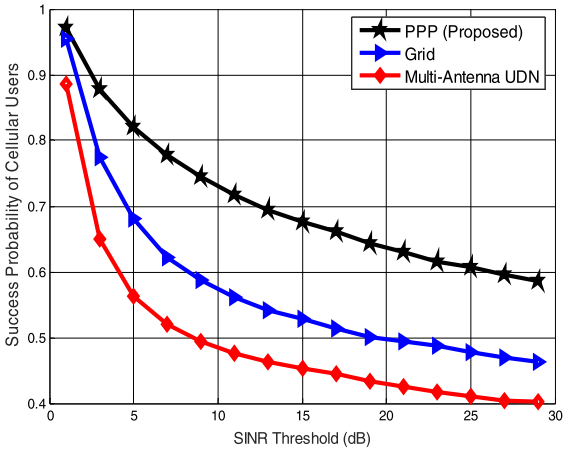

FIGURE 7. Success Probability of a Cellular User vs. the SINR Threshold.

CU_i are presented in Figure 7. Here, the probability of successful message exchange for the proposed PPP model is presented and compared with those of the square grid and conventional multi-antenna UDN approaches. According to Figure 7, as the SINR threshold values increase, the success probability gradually decreases if the fading distributions

are of exponential form. This result is due to the typical interferer signals (x_{R_j}, $x_{CU_j}$and x_{D_j}) from the interference links ($H_{R_jCU_i}$, $H_{CU_jCU_i}$ and $H_{D_jCU_i}$), as defined in equation 6. According to Figure 7, when the SINR threshold (τ_{CU}) is minimal (less than 2 dB), no substantial difference is observed among the approaches. A dramatic difference between the proposed PPP approach and the compared approaches (grid and multi-antenna UDN) gradually begins to appear at 3 dB and continues to grow. Improvements of 22% and 12% have been observed in the success probability compared with the multi-antenna UDN and grid approaches, respectively. Hence, the proposed PPP technique can maximize the success rate and yield enhanced robustness to all interferences at CU_i namely, RUI fromR_j, CCI from CU_j and CDI from D_j, as expressed in equation 6.

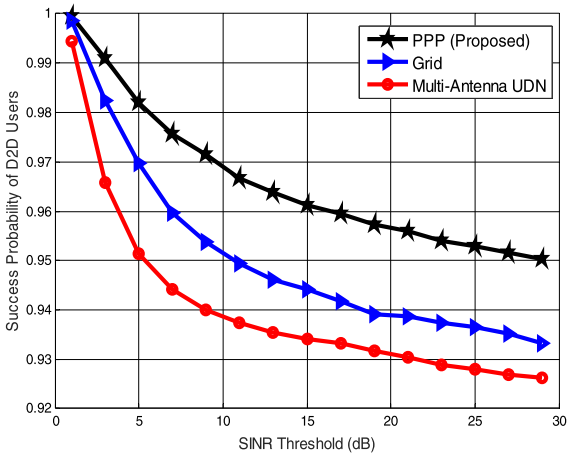

FIGURE 8. Success Probability of a D2D User vs. the SINR Threshold.

Furthermore, the results for the successful transmission for D2D user D_i are plotted for several SINR thresholds in Figure 8. The success probability with interferences ($P_{SUC_{D_i}}$) has been estimated in equation 34; however, the success probability after canceling the interferences $\left(P_{SUC(K)_{D_i}}\right)$ is expressed in equation 47. Figure 8 exhibits a similar pattern to Figure 7: lower values of the SINR threshold yield indistinguishable differences in $P_{SUC(K)_{D_i}}$; however, as τ_D increases, a consistent difference between the proposed PPP and the other two approaches is observed. At 30 dB, higher correlations of $P_{SUC(K)_{D_i}}$ of 0.928 and 0.932 are observed for the multi-antenna UDN and grid approaches, respectively. However, the proposed PPP method outperformed multi-antenna UDN by 1.93% and the grid approach by 2.3%. Hence, the proposed PPP approach outperforms the other approaches in canceling the interference at D2D users (D_iRUI from R_j, CCI from CU_j and CDI from D_j), as expressed in equation 47.

The ergodic capacity refers to the maximum rate of communication that can be achieved if the communication duration is sufficiently long to experience all channel states [76]. Figure 9 shows a plot of the ergodic capacity (in bits/second) with respect to the SINR threshold for the RN-to-CU hop,

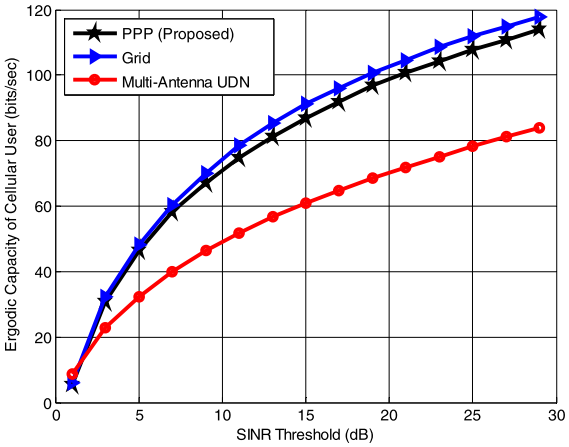

FIGURE 9. Ergodic Capacity of a Cellular User vs. the SINR Threshold.

as defined in equation 57. The Shannon–Hartley theorem has been used to calculate the ergodic capacity, which is expressed as $C = Bandwidth^* \log(1 + SINR_{th})$ in [77], [78]. A significant increment in the capacity ς_{RN-CU} with respect to τ_{CU} is observed among the grid, multi-antenna UDN, and proposed PPP approaches, this is due to the higher availability of bandwidth at CU_i. The grid approach achieves the highest overall ergodic capacity for all values of τ_{CU} among the compared approaches, which is due to the ideal deployment of BSs and RNs, as illustrated in Figure 5. The results show that when the SINR threshold is minimal (less than 3 dB), no significant differences are observed in the ergodic capacity values; however, when the SINR threshold starts to increase, the differences between the results are more readily observable. A close correlation of the ergodic capacity between the proposed PPP method and the grid model is observed with a small difference of 4% at an SINR threshold value of 13 dB. In addition, for an SINR threshold value of 30 dB, a massive improvement of 38% in the ergodic capacity of the proposed PPP method (112 bits/sec) is achieved compared with the multi-antenna UDN approach (83 bits/sec).

Moreover, the ergodic capacity of the D2D user $P_{SUC_{D_i}}$ for the CU-to-D2D hop is plotted against the SINR threshold in Figure 10, as expressed in equation 58. The results reveal a similar behavior of the ergodic capacity to that in Figure 9, where the grid model delivers a more accurate upper bound compared with the other approaches for all SINR values. However, a decrease is observed in the overall ergodic capacity values for the D2D user compared with CU. This result is due to the higher number of interferences, which results in low received signal values at D2D user D_i. The ergodic capacities are indistinguishable among the compared approaches for SINR thresholds of less than 3 dB; however, differences in ergodic values are observed for SINR values that exceed 5 dB. At 30 dB, the proposed PPP method exhibits ergodic capacity values that are close to those of the grid model and a 3.2% higher bit rate (17 bits/sec) than the multi-antenna UDN approach (15 bits/sec). According to these results, the proposed PPP method can reduce all channel interferences to increase the overall spectrum efficiency for D_i.

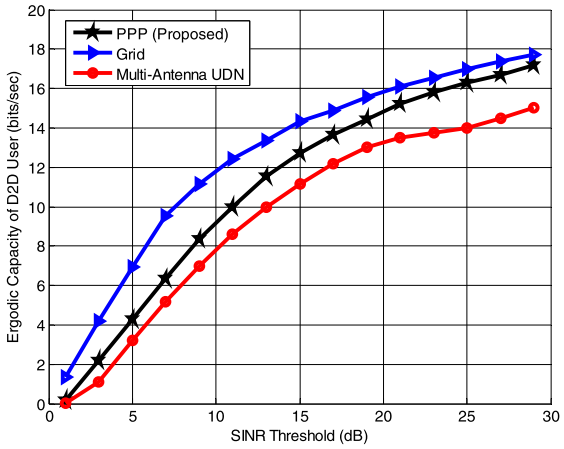

FIGURE 10. Ergodic Capacity of a D2D User vs. the SINR Threshold.

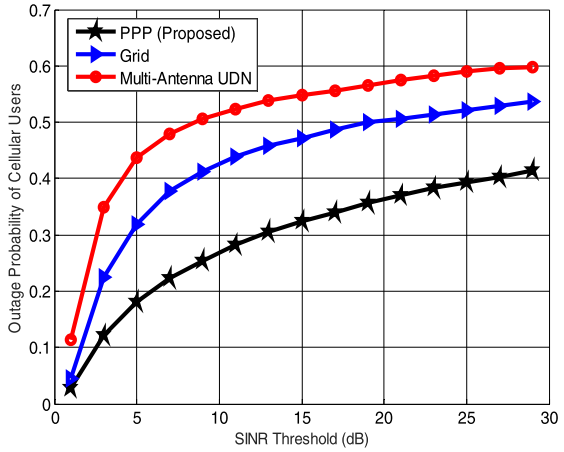

FIGURE 11. Outage Probability of a Cellular User vs. the SINR Threshold.

The outage probability is defined as the probability that $SINR_{CU_i}$ falls below a specified SINR threshold level, which is denoted as τ_{CU}. In Figure 11, the outage probability of CU is plotted against the SINR threshold for the proposed PPP method, the multi-antenna UDN, and the grid model. The outage probability is calculated as $P_{OUT_{CU_i}}(\tau_{CU}) \cong P\left(SINR_{CU_i} \leq \tau_{CU}\right)$, as defined in equation 51. The outage probabilities of all compared approaches for an SINR threshold value (τ_{CU}) that is below 2 dB are less than 10%; however, an increase in the outage probability is observed when τ_{CU} exceeds 3 dB. Significant differences in the outage probability values among all compared approaches are observed when τ_{CU} exceeds 5 dB. This phenomenon is due to the efficient user allocation performed based on users' SINRs rather than users' densities. The proposed PPP method achieved the lowest outage probability of 40% and outperformed the grid and multi-antenna UDN approaches by 12% and 18%, respectively.

Furthermore, the outage probabilities of D2D user D_i that were obtained for the proposed PPP method, multi-antenna UDN and grid model against various SINR threshold values are plotted in Figure 12. The outage probability of the D2D user has been evaluated via $P_{OUT_{D_i}}(\tau_D) \cong P\left(SINR_{D_i} \leq \tau_D\right)$, as expressed in equation 53. The pattern of the results

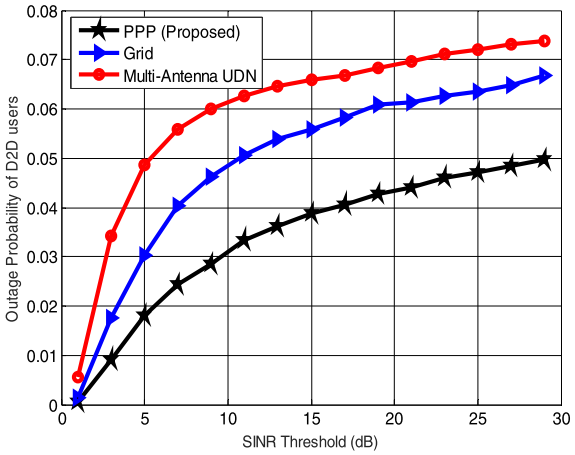

FIGURE 12. Outage Probability of a D2D User vs. the SINR Threshold.

presented in Figure 12 is analogous to those in Figure 11, namely, the proposed PPP method is successful in generating the lowest outage probability for D2D users compared with other approaches. The proposed PPP method consistently generates a lower outage probability for SINR threshold values (τ_D) that exceed 10 dB. The achieved outage probabilities for the proposed PPP approach are 15% and 23% lower compared with the grid and multi-antenna UDN approaches, respectively. These results demonstrate the performance of the proposed PPP method in mitigating cellular interference through improved user allocation based on users' SINRs rather than their density.

The number of users in a cell affects the overall performance of the users due to the occurrence of higher interferences among a large number of active cellular users. In this regard, the total success probabilities as functions of the node density for the proposed PPP method and the grid and multi-antenna UDN models are compared in Figure 13. The total success probability can be calculated as the scalar product of the individual capacities for all three hops, namely, BS-to-RN, RN-to-CU and CU-to-D2D, which can be expressed as $P_{T_{SUC(K)}} \cong P_{SUC(K)_{R_i}} \cdot P_{SUC(K)_{CU_i}} \cdot P_{SUC(K)_{D_i}}$, where $P_{SUC(K)_{R_i}}$, $P_{SUC(K)_{CU_i}}$ and $P_{SUC(K)_{D_i}}$ are defined in equations 41, 44 and 47, respectively. The total success probability decreases as the node density increases for all compared models. Moreover, among the three approaches, the proposed PPP model achieves the highest success probability (97%) for the minimum user density of 40 users/cell compared with the other two approaches. However, the achieved probabilities for the grid and multi-antenna UDN models reach approximately 94.3% and 93.1%, respectively, for the minimum of 40 users/cell and nearly 89% and 88%, respectively, for the maximum of 200 users/cell. These results verify the robustness of the proposed PPP approach for canceling the interferences at D_i (RUI from R_j, CCI from CU_j and CDI from D_j), as expressed in equation 47.

The total ergodic capacity for users is directly affected by the number of users who are present in a cell. More users

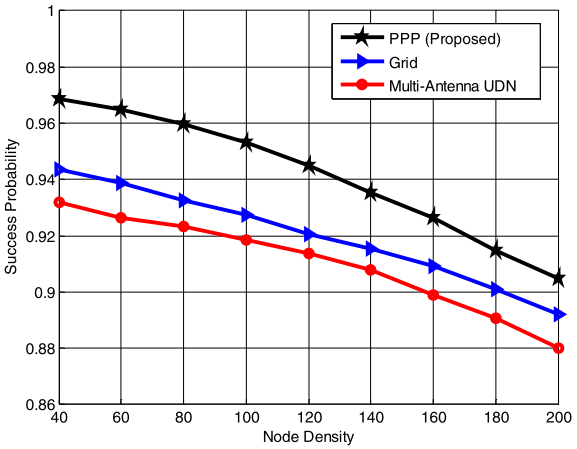

FIGURE 13. Success Probability vs. Node Density.

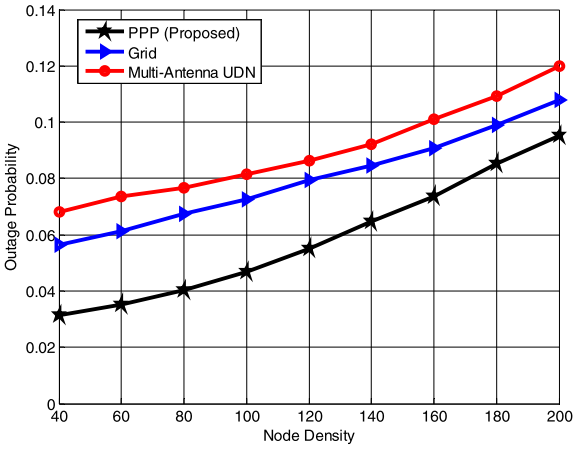

FIGURE 15. Outage Probability vs. User Density.

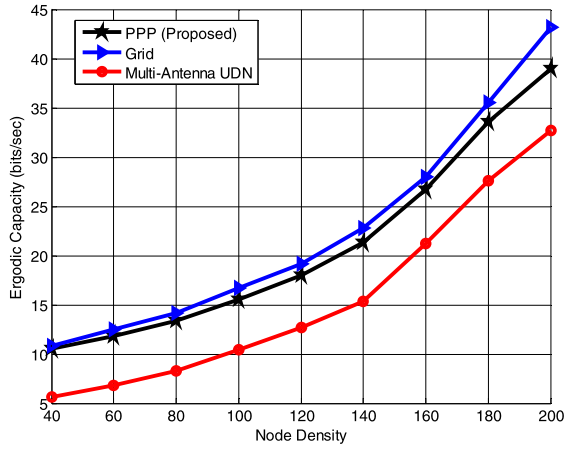

FIGURE 14. Ergodic Capacity vs. Node Density.

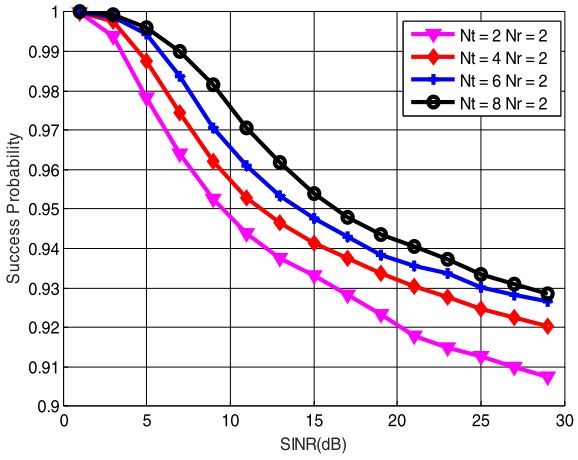

FIGURE 16. Success Probabilities under Various MIMO Conditions vs. the SINR Threshold.

correspond to a higher overall capacity due to a higher spectrum utilization and vice versa. Thus, the effect of the node density, namely, the number of users/cell, must be determined to validate the proposed PPP scheme. The total ergodic capacity, which is denoted as ς_T, is expressed in equation 59 as $\varsigma_T = \varsigma_{BS-RN} \cdot \varsigma_{RN-CU} \cdot \varsigma_{CU-D2D}$, which is the scalar product of the individual capacities that are achieved at R_i, CU_i and D_i. Figure 14 depicts the ergodic capacity as a function of the node density. The ergodic capacity increases with the node density for all approaches. The multi-antenna UDN model generates the lowest ergodic capacity with increasing node density. This observation is because the cells are designed according to the number of users who are present throughout the cell. Moreover, the results for the proposed PPP method are correlated to those for the grid model for a minimum node density of 40 users (11 bits/sec). The difference increases significantly to approximately 6% for the highest node density of 200 users, where the capacity value reaches 38 bits/sec and 44 bits/sec for the proposed PPP and grid models, respectively.

The outage probability that was achieved through the implementation of the proposed PPP method, compared with the grid and multi-antenna UDN approaches, is plotted in Figure 15. Similar behaviors of the outage probability as a function of the SINR threshold are observed, as illustrated in Figure 11 and Figure 12. The total outage probability, which is denoted as $P_{OUT(K)_T}(\tau)$, is expressed as $P_{OUT(K)_T}(\tau) = P_{OUT(K)_{R_i}}(\tau_R) \cdot P_{OUT(K)_{CU_i}}(\tau_{CU}) \cdot P_{OUT(K)_{D_i}}(\tau_D)$, as in equation 55, which is a scalar product of the individual probabilities that are achieved at R_i, CU_i and D_i, as expressed in equations 50, 51 and 54, respectively. The outage probability increases with the node density for all approaches; this is due to more devices being active in the cell, thereby causing higher interferences. The proposed PPP method consistently delivers a low outage probability that ranges from 2% to 9% for the minimum to maximum node densities, compared to the grid and multi-antenna UDN approaches, for which the probabilities range from 6% to 11% and 7% to 12%, respectively. Thus, the proposed PPP method can handle interference for both lower and higher node densities, thereby ensuring improved overall network performance.

The subsequent sections will further validate the performance of the proposed PPP method on different antenna configurations. As discussed, the total overall success

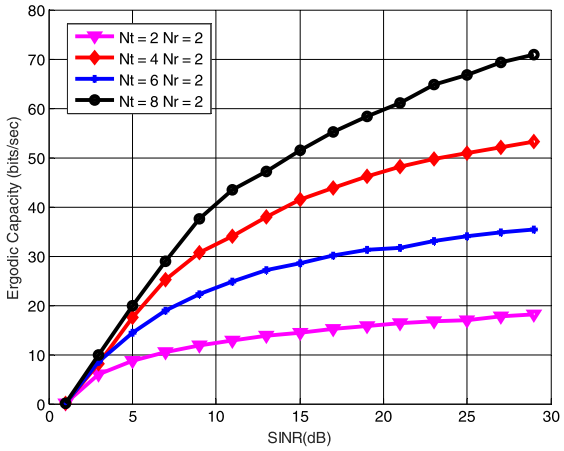

FIGURE 17. Ergodic Capacities under Various MIMO Conditions vs. the SINR Threshold.

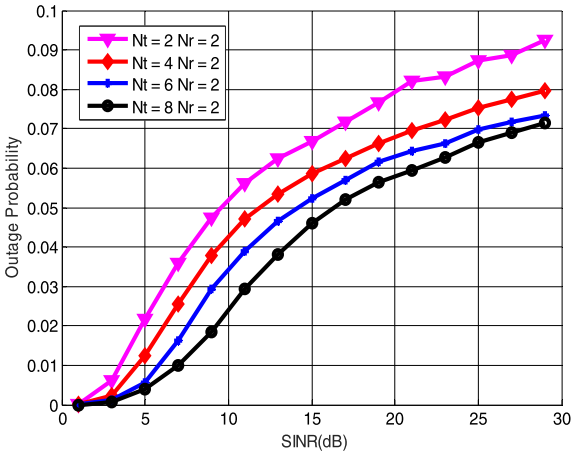

FIGURE 18. Outage Probabilities under Various MIMO Conditions vs. the SINR Threshold.

probability is affected by the number of transceiver antennas in the configuration, as expressed in equations 41, 44 and 47. Therefore, Figures 16, 17 and 18 investigate the behaviors of the success probability, ergodic capacity and outage probability, respectively, under various antenna configurations. Figure 16 plots the total success probability against various SINR threshold values by varying the number of transceiver antennas among, e.g., 2x2, 4x2, 6x2 and 8x2, where the first term represents N_t and N_r. The total success probability decreases as the SINR threshold value decreases, similar to Figure 7 and Figure 8. The total success probability is nearly ideal for SINR threshold values of less than 3 dB, regardless of the antenna configuration. A difference in the values of the total success probability is observed when the SINR threshold value reaches 5 dB and higher. $N_t = 8$ corresponds to the highest success probability, followed by $N_t = 6$ and $N_t = 4$, and $N_t = 2$ corresponds to the lowest total success probability. The total difference between the highest total success probability of $N_t = 8$ and the lowest total success probability $N_t = 2$ is 3.3%. The results clearly show that the proposed PPP approach supports the MIMO configuration efficiently and that deploying multiple antennas for the transmission increases the spectral efficiency, thereby yielding a higher successful transmission rate.

The total ergodic capacity is calculated as the scalar product of the individual ergodic capacities that are achieved at R_i, CU_i and D_i, as estimated in equation 59. However, the capacities for individual hops, namely, ς_{BS-RN}, ς_{RN-CU}, and ς_{CU-D2D}, are calculated via equations 56, 57, and 58, respectively. Figure 17 plots the total ergodic capacity against various SINR threshold values for various antenna configurations. The total ergodic capacity increases with the SINR threshold value, similar to Figure 9 and Figure 10. The total ergodic capacity is very low for all antenna configurations for SINR threshold values of less than 3 dB. However, as the SINR value increases, the achieved total ergodic capacity also increases, and the difference becomes distinguishable between the antenna configurations. At a SINR threshold of 30 dB, $N_t = 8$ corresponds to the highest total ergodic capacity (71 bits/sec), followed by $N_t = 6$ (53 bits/sec), $N_t = 4$ (36 bits/sec), and $N_t = 2$ (19 bits/sec). This observation validates that when the number of pairs of transmitter and receiver antennas is increased in the system, coupled with the proposed PPP technique, spatial multiplexing can be increased, thereby enhancing the overall ergodic capacity of the system.

The total outage probability is calculated in equation 55 as the scalar product of the outage probabilities of individual hops R_i ($P_{OUT(K)_{R_i}}$), CU_i ($P_{OUT(K)_{CU_i}}$), and D_i ($P_{OUT(K)_{D_i}}$), which are expressed in equations 50, 52 and 54, respectively. Figure 18 depicts the outage probabilities under various antenna configurations against various SINR threshold values. The total outage probability increases with the SINR threshold value, similar to Figure 11 and Figure 12. As expected, the 8x2 antenna configuration delivers the best performance while achieving the minimum outage probability of 7% at an SINR threshold value of 30 dB. A maximum total outage probability of 9.3% is achieved by the 2x2 antenna configuration at an SINR threshold value of 30 dB, followed by 4x2 (8%), 6x2 (7.2%) and 8x2 (7%). The difference between the total outage probabilities for $N_t = 2$ and $N_t = 8$ is 33%. This observation confirms that deploying the multiple antenna configurations at the transceivers for the proposed PPP model enhances the spectrum efficiency, which leads to the realization of the optimal total outage probability.

VII. CONCLUSIONS

Next-generation wireless systems, such as 5G and beyond, are expected to implement efficient interference management mechanisms to achieve more reliable communications. D2D and cellular links share similar spectrum resources, which causing severe interference between them. Therefore, interference management is crucial because interference severely hinders the overall network performance. In this paper, a stochastic-geometry-based PPP model is designed and

a comparative approach is used to implement the realistic positioning of BS, RN, CU, and D2D users, with the objective of realizing interference-free D2D-enabled cellular networks. The success probabilities, ergodic capacities and outage probabilities that are achieved by the cellular and D2D users as functions of the SINR threshold and node density are examined. Moreover, these results have been elaborated at various MIMO antenna configurations to validate the results. The numerical results confirm the robustness of the proposed PPP model against interference for the D2D-enabled cooperative cellular network compared with the grid and multi-antenna UDN models. The results that are presented in this paper can be used to conveniently evaluate and implement future-generation 5G communication networks for real-life environments. In future work, the influence of cellular and D2D users' mobility factors will be investigated. Moreover, severe undesired signals, such as device noise and adjacent-channel interference, should be incorporated into the model and mitigated. In addition, there are several other nodes distribution approaches such as the Matern cluster process (MCP) and Matern hard-core process (MHCP) with a minimum inter-distance between every two nodes, which can be used for more realistic modeling.

APPENDIX A

The success probability of the first hop is calculated as

$$P_{SUC_{R_i}} \cong P\left(\frac{\rho_{BS_i} \mathrm{P}_{L,M} \alpha_i^{-\gamma} \left\|H_{BS_iR_i}\right\|^2}{\mathrm{I}_{R_i}} \geq \tau_R\right) \tag{60}$$

$$P_{SUC_{R_i}} \cong P\left(\left\|H_{BS_iR_i}\right\|^2 \geq \tau_R \rho_{BS_i}^{-1} \mathrm{P}_{L,M}^{-1} \alpha_i^{\gamma} \mathrm{I}_{R_i}\right) \tag{61}$$

where $\mathrm{I}_{R_i}$is defined in equation 3 as the overall interference received at R_1 i.e.,

$$\mathrm{I}_{R_i} = \sqrt{\rho_{R_i}} \left\|H_{R_iR_i}\right\| x_{R_i} + \sum_{x_{Rj} \in \psi_R} \sqrt{\rho_{R_j}} \mathrm{P}_{L,RR} \alpha^{-\frac{\gamma}{2}} \left\|H_{R_jR_i}\right\| x_{R_j} \tag{62}$$

Let us define $f_{\mathrm{I}_{R_i}}(t) = dP\left(\mathrm{I}_{R_i} < t\right)$ as the PDF of I_{R_i}. The integration of $f_{\mathrm{I}_{R_i}}(t)$using the CCDF $F_{R_i}^c(t)$ transforms it as

$$\Delta(s)_{SR} \cong \int_0^{\infty} F_{SR}^{C}(st) \cdot f_{I_{T,R_1}}(t)\, dt \tag{63}$$

Note that, the power of the desired signal is distributed as $\left\|H_{BS_iR_i}\right\|^2 \succ X_i^{\infty_{N_R}}$, and the probability of success given is by

$$\begin{aligned} P_{SUC_{R_i}} &\cong P\left(SINR_{R_i} \geq \tau_R\right) \\ &\cong P\left(\left\|H_{BS_iR_i}\right\|^2 \geq \tau_R \rho_{BS_i}^{-1} \mathrm{P}_{L,M}^{-1} \alpha_i^{\gamma} \mathrm{I}_{R_i}\right) && (64) \\ &\cong \int_0^{\infty} F_{R_i}^c(st) \cdot f_{\mathrm{I}_{R_i}}(t) dt && (65) \\ &\cong \Delta(s)\|_{s=\tau_R \rho_{BS_i}^{-1} \mathrm{P}_{L,M}^{-1} \alpha_i^{\gamma}} && (66) \end{aligned}$$

Finally, using the CCDF $F_{R_i}^c(st) = e^{-t}$ and Laplace transform, the success probability can be expressed using the transformation of $f_{\mathrm{I}_{R_i}}(t)$ as

$$\Delta(s) \cong \int_0^{\infty} F_{R_i}^c(st) \cdot f_{\mathrm{I}_{R_i}}(t) dt \tag{67}$$

$$\zeta\left\{f_{\mathrm{I}_{R_i}}(t)\right\}(s) = \xi_{\mathrm{I}_{R_i}}(s) \tag{68}$$

Finally, using the CCDF $F_{R_i}^c(st) = \bigcup_n e^{-nt} \bigcup_i e^{a_n t^i}$, the transformation of $f_{\mathrm{I}_{R_i}}(t)$ is given by

$$\Delta(s) \cong \int_0^{\infty} F_{R_i}^c(st) \cdot f_{\mathrm{I}_{R_i}}(t) dt \tag{69}$$

$$\Delta(s) \cong \int_0^{\infty} \left[\bigcup_n e^{-nt} \bigcup_i e^{a_n (st)^i}\right] \cdot f_{\mathrm{I}_{R_i}}(t) dt \tag{70}$$

$$\Delta(s) \cong \bigcup_n \bigcup_i a_n (st)^i \left\{\int_0^{\infty} \left(e^{-nt} t^i\right) \cdot \left(f_{\mathrm{I}_{R_i}}(t) dt\right)\right\} \tag{71}$$

$$\Delta(s) \cong \bigcup_n \bigcup_i a_n s^i \left[\xi\left(t^i \cdot f_{\mathrm{I}_{R_i}}(t)\right)\right][ns] \tag{72}$$

$$\Delta(s) \cong \bigcup_n \bigcup_i \left\{a_n (-s)^i \frac{d^i}{d(ns)^i} \cdot \xi_{\mathrm{I}_{R_i}}(ns)\right\} \tag{73}$$

$$\Delta(s) \cong \bigcup_n \bigcup_i \left\{a_n \left(\frac{-s}{n}\right)^i \frac{d^i}{d(s)^i} \cdot \xi_{\mathrm{I}_{R_i}}(ns)\right\} \tag{74}$$

where equation 18 is obtained using the Laplace transform property $t^n f(t) \leftrightarrow (-1)^n \frac{d^n}{ds^n} \cdot \xi[f(t)]s$ [79]. Using the moment-generating function of $X_i^{\infty_{N_R}}$and Gamma distributions, and applying it to [80] (Theorem. 1) we can obtain equation 16.

APPENDIX B

Building on [80] (Theorem. 3), we obtain $\alpha(s)$ in equation 18 bounded as $\alpha(s) \in \left[\alpha^{\max}(s), \alpha^{\min}(s)\right]$, where $\alpha^{\max}(s)$ and $\alpha^{\min}(s)$ are defined in equation iv and equation v, respectively. Then, the lower and upper bounds on $\xi_{\mathrm{I}_{R_i}}(s)$ as shown in equation i, are readily defined in equation ii and equation iii.

APPENDIX C

The success probability of the RN-to-CU hop is calculated as

$$P_{SUC_{CU_i}} \cong P\left(SINR_{CU_i} \geq \tau_{CU}\right) \tag{75}$$

$$P_{SUC_{CU_i}} \cong P\left(\frac{\rho_{R_i} \mathrm{P}_{L,O} h_i^{-\gamma} \left\|H_{R_iCU_i}\right\|^2}{\mathrm{I}_{CU_i}} \geq \tau_{CU}\right) \tag{76}$$

$$P_{SUC_{CU_i}} \cong P\left(\left\|H_{R_iCU_i}\right\|^2 \geq \tau_{CU} \rho_{R_i}^{-1} \mathrm{P}_{L,O}^{-1} h_i^{\gamma} \mathrm{I}_{CU_i}\right) \tag{77}$$

where I_{CU_i} is defined in equation 6 as

$$\begin{aligned} \mathrm{I}_{CU_i} = &\sum_{x_{Rj} \in \psi_R} \sqrt{\rho_{R_j}} \mathrm{P}_{L,O} h^{-\frac{\gamma}{2}} \left\|H_{R_jCU_i}\right\| x_{R_j} \\ &+ \sum_{x_{CU_j} \in \psi_{CU}} \sqrt{\rho_{CU_j}} \mathrm{P}_{L,P} f^{-\frac{\gamma}{2}} \left\|H_{CU_jCU_i}\right\| x_{CU_j} \\ &+ \sum_{x_{Dj} \in \psi_D} \sqrt{\rho_{D_j}} \mathrm{P}_{L,N} g^{-\frac{\gamma}{2}} \left\|H_{D_jCU_i}\right\| x_{D_j} \end{aligned} \tag{78}$$

The desired signal is distributed as $\left\|H_{R_iCU_i}\right\|^2 \succ X_i^{\infty_{N_{CU}}}$. In contrast, the moment generating function of the $X_1^{2_{N_{R,R}}}$ distribution can provide the Laplace transform of I_{CU_i} [68] (Page. 125) and can be computed as

$$\xi_{\mathrm{I}_{CU_i}}(s) \cong \bar{E}\left(\prod_{i\in\psi_{CU}} \bar{E}\left\{\exp\left(-s\frac{\rho_{R_i}}{N_R}\mathrm{P}_{L,O}h_i^{-\gamma}\left\|H_{R_iCU_i}\right\|^2\right)\right\}\right) \tag{79}$$

APPENDIX D

A cellular user is located at the origin Θ_{CU_i}, and a D2D user is situated at Θ_{D_i}. Since a D2D user is communicating with the nearest another D2D user, the CDF of D_i can be calculated by,

$$\begin{aligned} &P\left(\check{\mathrm{d}}_{CU-D2D} \geq \Theta_{D_i}\right) \\ &\quad \cong 1 - P\left(\textit{no cellular user closer than } \Theta_{D_i}\right) \quad (80) \\ &\quad \cong 1 - e^{\left(-\pi\Upsilon_D\Theta_{D_i}\right)} \quad (81) \end{aligned}$$

Then the PDF of $\check{\mathrm{d}}_{CU-D2D}$ is $f\left(\check{\mathrm{d}}_{CU-D2D}\right) = e^{-\pi\Upsilon_D\Theta_{D_i}^2\check{\mathrm{d}}_{CU-D2D}} 2\pi\Upsilon_D\check{\mathrm{d}}_{CU-D2D}$, which yields its SINR as stated in [64]. The CDF of SINR regarding the I_{D_i} is given by,

$$Z_{D_i}(\tau) = 1 - \Xi\left[P\left(SINR_{D_i} \geq \tau_D\right)\right] \tag{82}$$

$$\begin{aligned} Z_{D_i}(\tau) = 1 - \int_0^\infty & 2\pi\Upsilon_D\check{\mathrm{d}}_{CU-D2D}e^{-\pi\Upsilon_D\Theta_{D_i}^2\check{\mathrm{d}}_{CU-D2D}} \\ & \cdot P\left(\frac{\rho_{CU_i}\mathrm{P}_{L,N}f_i^{-\gamma}\left\|H_{CU_iD_i}\right\|^2}{\mathrm{I}_{D_i}+n_{D_i}} \geq \tau_D\right) \\ & \cdot d\left(\check{d}_{CU-D2D}\right) \end{aligned} \tag{83}$$

$$\begin{aligned} Z_{D_i}(\tau) = 1 - \int_0^\infty & 2\pi\Upsilon_D\check{\mathrm{d}}_{CU-D2D}e^{-\pi\Upsilon_D\Theta_{D_i}^2\check{\mathrm{d}}_{CU-D2D}} \cdot \\ & P\left(\left\|H_{CU_iD_i}\right\|^2 \geq \frac{\tau_D\mathrm{P}_{L,N}^{-1}f_i^{\gamma}\mathrm{I}_{D_i}}{\rho_{CU_i}} + n_{D_i}\right) \\ & \cdot d\left(\check{\mathrm{d}}_{CU-D2D}\right) \end{aligned} \tag{84}$$

$$\begin{aligned} Z_{D_i}(\tau) = 1 - \int_0^\infty & 2\pi\Upsilon_D\check{\mathrm{d}}_{CU-D2D}e^{-\pi\Upsilon_D\Theta_{D_i}^2\check{\mathrm{d}}_{CU-D2D}} \\ & \times \Xi\left\{e^{-\frac{\tau_D\mathrm{P}_{L,N}^{-1}f_i^{\gamma}}{\rho_{CU_i}}\left(\mathrm{I}_{D_i}+n_{D_i}\right)}\right\} \cdot d\left(\check{\mathrm{d}}_{CU-D2D}\right) \end{aligned} \tag{85}$$

$$\begin{aligned} Z_{D_i}(\tau) = 1 - \int_0^\infty & 2\pi\Upsilon_D\check{\mathrm{d}}_{CU-D2D} \\ & \times e^{-\pi\Upsilon_D\Theta_{D_i}^2\check{\mathrm{d}}_{CU-D2D}\left(\frac{\tau_D\mathrm{P}_{L,N}^{-1}f_i^{\gamma}n_{D_i}}{\rho_{CU_i}}\right)}\xi_{\mathrm{I}_{D_i}} \\ & \times \left(\frac{\tau_D\mathrm{P}_{L,N}^{-1}f_i^{\gamma}}{\rho_{CU_i}}\right) \cdot d\left(\check{\mathrm{d}}_{CU-D2D}\right) \end{aligned} \tag{86}$$

$$\xi_{\mathrm{I}_{D_i}}(s) = \Xi\left[e^{\left\{\left(\frac{\tau_D\mathrm{P}_{L,N}^{-1}f_i^{\gamma}}{\rho_{CU_i}}\right)\left(-\frac{\rho_{CU_i}}{N_{D2D}}\right)\right\}\prod_{i=1}^{N_{D2D}}\left\|H_{CU_iD_i}\right\|}\right] \tag{87}$$

We using the fact that $\left\|H_{CU_iD_i}\right\|^2 = \prod_{i=1}^{N_{D2D}}\left\|H_{CU_iD_i}\right\|$ with $f_i \succ \exp(1)$, which simplifies to

$$\xi_{\mathrm{I}_{D_i}}(s) = \Xi\left\{\prod_{i=1}^{N_{D2D}}\Xi_{f_i^{\gamma}}\left[e^{\left(\frac{\tau_D\mathrm{P}_{L,N}^{-1}}{\rho_{CU_i}}\right)\left(-\frac{\rho_{CU_i}}{N_{D2D}}\right)(f_i^{\gamma})}\right]\right\} \tag{88}$$

$$\zeta_{I_{T,R_1}}(s) = \Xi\left\{\prod_{i=1}^{N_{D2D}}\frac{1}{1+\left(\frac{\tau_D\mathrm{P}_{L,N}^{-1}}{\rho_{CU_i}}\right)\left(-\frac{\rho_{CU_i}}{N_{D2D}}\right)}\right\} \tag{89}$$

The probability generating function of the PPP of D2D users with interference I_{D_i}states that functions $\psi_D(x)$ are denoted by

$$\bar{E}\left[\prod_{i=1}^{N_{D2D}}\psi_D(x)\right] = \exp\left(-\mathrm{I}_{D_i}\int_{\Theta_D^2}\left(1-\psi_D(x)\right)dx\right) \tag{90}$$

The probability of generating the function of the $\zeta_{I_{T,R_1}}(s)$ yields,

$$\xi_{\mathrm{I}_{D_i}}(s) = \exp\left(-2\pi\mathrm{I}_{D_i}\int_{\check{\mathrm{d}}_{CU-D2D}}^{\infty}\left(1-\frac{1}{1+\frac{\tau_D\mathrm{P}_{L,N}^{-1}f_i^{\gamma}}{\rho_{CU_i}}x}\right)xdx\right) \tag{91}$$

REFERENCES

[1] R. El Hattachi and J. Erfanian, "5G white paper," Next Generation Mobile Networks, NGMN. Alliance, white paper, 2015, pp. 1–125. [Online]. Available: https://www.ngmn.org/fileadmin/ngmn/content/images/news/ngmn_news/NGMN_5G_White_Paper_V1_0.pdf

[2] J. G. Andrews *et al.*, "What will 5G be?" *IEEE J. Sel. Areas Commun.*, vol. 32, no. 6, pp. 1065–1082, May 2014.

[3] S. Patel, M. Chauhan, and K. Kapadiya, "5G: Future mobile technology-vision 2020," *Int. J. Comput. Appl.*, vol. 54, no. 17, pp. 1–5, Jan. 2012.

[4] A. Al-Samman, M. Hindia, and T. Rahman, "Path loss model in outdoor environment at 32 GHz for 5G system," in *Proc. IEEE 3rd Int. Symp. Telecommun. Technol. (ISTT)*, Nov. 2016, pp. 9–13.

[5] S. Weber, J. G. Andrews, and N. Jindal, "An overview of the transmission capacity of wireless networks," *IEEE Trans. Commun.*, vol. 58, no. 12, pp. 3593–3604, Dec. 2010.

[6] S. Talwar, D. Choudhury, K. Dimou, E. Aryafar, B. Bangerter, and K. Stewart, "Enabling technologies and architectures for 5G wireless," in *IEEE MTT-S Int. Microw. Symp. Dig.*, Jun. 2014, pp. 1–4.

[7] F. Qamar, T. Abbas, M. N. Hindia, K. B. Dimyati, K. A. B. Noordin, and I. Ahmed, "Characterization of MIMO propagation channel at 15 GHz for the 5G spectrum," in *Proc. IEEE 13th Malaysia Int. Conf. Commun. (MICC)*, Nov. 2017, pp. 265–270.

[8] T. Abbas, F. Qamar, I. Ahmed, K. Dimyati, and M. B. Majed, "Propagation channel characterization for 28 and 73 GHz millimeter-wave 5G frequency band," in *Proc. IEEE 15th Conf. Res. Develop. (SCOReD)*, Dec. 2017, pp. 297–302.

[9] F. Qamar, M. H. S. Siddiqui, K. Dimyati, K. A. B. Noordin, and M. B. Majed, "Channel characterization of 28 and 38 GHz MM-wave frequency band spectrum for the future 5G network," in *Proc. IEEE 15th Conf. Res. Develop. (SCOReD)*, Dec. 2017, pp. 291–296.

[10] T. E. Bogale and L. B. Le, "Massive MIMO and mmWave for 5G wireless HetNet: Potential benefits and challenges," *IEEE Veh. Technol. Mag.*, vol. 11, no. 1, pp. 64–75, Mar. 2016.

[11] M. N. Hindia, M. M. Fadoul, T. A. Rahman, and I. S. Amiri, "A stochastic geometry approach to full-duplex MIMO relay network," in *Proc. Wireless Commun. Mobile Comput.*, Jan. 2018, Art. no. 8342156.

[12] F. Qamar, K. B. Dimyati, M. N. Hindia, K. A. B. Noordin, and A. M. Al-Samman, "A comprehensive review on coordinated multi-point operation for LTE-A," *Comput. Netw.*, vol. 123, pp. 19–37, Aug. 2017.
[13] K. M. Modieginyane, B. B. Letswamotse, R. Malekian, and A. M. Abu-Mahfouz, "Software defined wireless sensor networks application opportunities for efficient network management: A survey," *Comput. Elect. Eng.*, vol. 66, pp. 274–287, Feb. 2018.
[14] X. Zhang, W. Cheng, and H. Zhang, "Heterogeneous statistical QoS provisioning over 5G mobile wireless networks," *IEEE Netw.*, vol. 28, no. 6, pp. 46–53, Nov. 2014.
[15] O. Elijah, T. A. Rahman, I. Orikumhi, C. Y. Leow, and M. N. Hindia, "An overview of Internet of things (IoT) and data analytics in agriculture: Benefits and challenges," *IEEE Internet Things J.*, vol. 5, no. 5, pp. 3758–3773, Oct. 2018.
[16] C. X. Mavromoustakis, G. Mastorakis, and J. MongayBatalla, Eds., *Internet of Things (IoT) in 5G Mobile Technologies*, vol. 8. Cham, Switzerland: Springer, 2016. [Online]. Available: https://link.springer.com/book/10.1007%2F978-3-319-30913-2. doi: 10.1007/978-3-319-30913-2.
[17] D. Udeshi and F. Qamar, "Quality analysis of epon network for uplink and downlink design," *Asian J. Eng., Sci. Technol.*, vol. 4, no. 2, pp. 1–6, Sep. 2014.
[18] I. A. T. Hashem, I. Yaqoob, N. B. Anuar, S. Mokhtar, A. Gani, and S. U. Khan, "The rise of 'big data' on cloud computing: Review and open research issues," *Inf. Syst.*, vol. 47, pp. 98–115, Jan. 2015.
[19] A. Gachhadar, M. N. Hindia, F. Qamar, M. H. S. Siddiqui, K. A. Noordin, and I. S. Amiri, "Modified genetic algorithm based power allocation scheme for amplify-and-forward cooperative relay network," *Comput. Elect. Eng.*, vol. 69, pp. 628–641, Jul. 2018.
[20] K. A. B. Noordin, M. N. Hindia, F. Qamar, and K. Dimyati, "Power allocation scheme using PSO for amplify and forward cooperative relaying network," in *Proc. Sci. Inf. Conf.*, Nov. 2018, pp. 636–647.
[21] M. N. Hindia, F. Qamar, M. B. Majed, T. A. Rahman, and I. S. Amiri, "Enabling remote-control for the power sub-stations over LTE-A networks," *Telecommun. Syst.*, vol. 70, pp. 37–53, Jan. 2018.
[22] I. F. Akyildiz, S. Nie, S.-C. Lin, and M. Chandrasekaran, "5G roadmap: 10 key enabling technologies," *Comput. Netw.*, vol. 106, pp. 17–48, Sep. 2016.
[23] R. Baldemair *et al.*, "Ultra-dense networks in millimeter-wave frequencies," *IEEE Commun. Mag.*, vol. 53, no. 1, pp. 202–208, Jan. 2015.
[24] X. Zhu, J. Zeng, X. Su, C. Xiao, J. Wang, and L. Huang, "On the virtual cell transmission in ultra dense networks," *Entropy*, vol. 18, no. 10, p. 374, 2016.
[25] A. Gupta and R. K. Jha, "A survey of 5G network: Architecture and emerging technologies," *IEEE Access*, vol. 3, pp. 1206–1232, 2015.
[26] H. Zhang, N. Liu, X. Chu, K. Long, A.-H. Aghvami, and V. C. Leung, "Network slicing based 5G and future mobile networks: Mobility, resource management, and challenges," *IEEE Commun. Mag.*, vol. 55, no. 8, pp. 138–145, Aug. 2017.
[27] H. H. Hussein and S. M. A. El-Kader, "Enhancing signal to noise interference ratio for device to device technology in 5G applying mode selection technique," in *Proc. Int. Conf. Adv. Control Circuits Syst. (ACCS)*, Nov. 2017, pp. 187–192.
[28] N.-P. Nguyen, T. Q. Duong, H. Q. Ngo, Z. Hadzi-Velkov, and L. Shu, "Secure 5G wireless communications: A joint relay selection and wireless power transfer approach," *IEEE Access*, vol. 4, pp. 3349–3359, 2016.
[29] R. Pabst *et al.*, "Relay-based deployment concepts for wireless and mobile broadband radio," *IEEE Commun. Mag.*, vol. 42, no. 9, pp. 80–89, Sep. 2004.
[30] J. A. Aldhaibani, A. Yahya, and R. B. Ahmad, "Coverage extension and balancing the transmitted power of the moving relay node at LTE-A cellular network," *Sci. World J.*, vol. 2014, 2014, Art. no. 815720. [Online]. Available: https://www.hindawi.com/journals/tswj/2014/815720/abs/. doi: 10.1155/2014/815720.
[31] S.-W. Jeon and M. Gastpar, "A survey on interference networks: Interference alignment and neutralization," *Entropy*, vol. 14, no. 10, pp. 1842–1863, 2012.
[32] V. N. Q. Bao and H. Y. Kong, "Performance analysis of decode-and-forward relaying with partial relay selection for multihop transmission over Rayleigh fading channels," *J. Commun. Netw.*, vol. 12, no. 5, pp. 433–441, Oct. 2010.
[33] R. J. Roden and D. Tayler, "Frame relay networks," *Digit. Tech. J.*, vol. 5, no. 1, p. 647, 1993.
[34] J. Qiao, X. S. Shen, J. W. Mark, Q. Shen, Y. He, and L. Lei, "Enabling device-to-device communications in millimeter-wave 5G cellular networks," *IEEE Commun. Mag.*, vol. 53, no. 1, pp. 209–215, Jan. 2015.
[35] F. Boccardi, R. W. Heath, A. Lozano, T. L. Marzetta, and P. Popovski, "Five disruptive technology directions for 5G," *IEEE Commun. Mag.*, vol. 52, no. 2, pp. 74–80, Feb. 2014.
[36] H.-S. Liao, P.-Y. Chen, and W.-T. Chen, "An efficient downlink radio resource allocation with carrier aggregation in LTE-advanced networks," *IEEE Trans. Mobile Comput.*, vol. 13, no. 10, pp. 2229–2239, Oct. 2014.
[37] S. Rostami, K. Arshad, and P. Rapajic, "Aggregation-based spectrum assignment in cognitive radio networks," in *Proc. Int. Conf. Adv. Comput. Commun. Syst.*, Dec. 2013, pp. 1–6.
[38] H. R. Chayon, K. Dimyati, H. Ramiah, and A. W. Reza, "An improved radio resource management with carrier aggregation in LTE advanced," *Appl. Sci.*, vol. 7, no. 4, p. 394, 2017.
[39] S. Rostami, K. Arshad, and P. Rapajic, "A joint resource allocation and link adaptation algorithm with carrier aggregation for 5G LTE-Advanced network," in *Proc. 22nd Int. Conf. Telecommun. (ICT)*, Apr. 2015, pp. 102–106.
[40] Z. Zhou, K. Ota, M. Dong, and C. Xu, "Energy-efficient matching for resource allocation in D2D enabled cellular networks," *IEEE Trans. Veh. Technol.*, vol. 66, no. 6, pp. 5256–5268, Jun. 2017.
[41] H. A. U. Mustafa, M. A. Imran, M. Z. Shakir, A. Imran, and R. Tafazolli, "Separation framework: An enabler for cooperative and D2D communication for future 5G networks," *IEEE Commun. Surveys Tuts.*, vol. 18, no. 1, pp. 419–445, 1st Quart., 2016.
[42] H. Benn, "Vision and key features for 5th generation (5G) cellular," Samsung R&D Institute UK, Staines, U.K., Tech. Rep., 2014. [Online]. Available: http://cambridgewireless.co.uk/Presentation/RadioTech_30.01.14_HowardBenn.Samsung.pdf
[43] A. Asadi and V. Mancuso, "Network-assisted outband D2D-clustering in 5G cellular networks: Theory and practice," *IEEE Trans. Mobile Comput.*, vol. 16, no. 8, pp. 2246–2259, Aug. 2017.
[44] J. G. Andrews, A. K. Gupta, and H. S. Dhillon. (2016). "A primer on cellular network analysis using stochastic geometry." [Online]. Available: https://arxiv.org/abs/1604.03183
[45] H. M. Taylor and S. Karlin, *An Introduction to Stochastic Modeling*. New York, NY, USA: Academic, 2014.
[46] H. P. Keeler, "Notes on the Poisson point process," Weierstrass Inst., Berlin, Germany, Tech. Rep., 2016. [Online]. Available: https://hpaulkeeler.com/wp-content/uploads/2018/08/PoissonPointProcess.pdf
[47] W. Dargie and A. Schill, "Stability and performance analysis of randomly deployed wireless networks," *J. Comput. Syst. Sci.*, vol. 77, no. 5, pp. 852–860, Sep. 2011.
[48] H. ElSawy, E. Hossain, and M. Haenggi, "Stochastic geometry for modeling, analysis, and design of multi-tier and cognitive cellular wireless networks: A survey," *IEEE Commun. Surveys Tuts.*, vol. 15, no. 3, pp. 996–1019, 3rd Quart., 2013.
[49] D. Dobkin and D. Silver, "Applied computational geometry: Towards robust solutions of basic problems," *J. Comput. Syst. Sci.*, vol. 40, no. 1, pp. 70–87, Feb. 1990.
[50] I. Flint, H.-B. Kong, N. Privault, P. Wang, and D. Niyato, "Analysis of heterogeneous wireless networks using Poisson hard-core hole process," *IEEE Trans. Wireless Commun.*, vol. 16, no. 11, pp. 7152–7167, Nov. 2017.
[51] S. Kajioka, N. Wakamiya, and M. Murata, "Autonomous and adaptive resource allocation among multiple nodes and multiple applications in heterogeneous wireless networks," *J. Comput. Syst. Sci.*, vol. 78, no. 6, pp. 1673–1685, Nov. 2012.
[52] J. G. Andrews, F. Baccelli, and R. K. Ganti, "A tractable approach to coverage and rate in cellular networks," *IEEE Trans. Commun.*, vol. 59, no. 11, pp. 3122–3134, Nov. 2011.
[53] M. Dehghani, K. Arshad, and R. MacKenzie, "LTE-Advanced radio access enhancements: A survey," *Wireless Pers. Commun.*, vol. 80, no. 3, pp. 891–921, Feb. 2015.
[54] M. Salehi, A. Mohammadi, and M. Haenggi, "Analysis of D2D underlaid cellular networks: SIR meta distribution and mean local delay," *IEEE Trans. Commun.*, vol. 65, no. 7, pp. 2904–2916, Jul. 2017.
[55] S. Andreev, O. Galinina, A. Pyattaev, K. Johnsson, and Y. Koucheryavy, "Analyzing assisted offloading of cellular user sessions onto D2D links in unlicensed bands," *IEEE J. Sel. Areas Commun.*, vol. 33, no. 1, pp. 67–80, Jan. 2015.
[56] Z. Zhang, R. Q. Hu, Y. Qian, A. Papathanassiou, and G. Wu, "D2D communication underlay uplink cellular network with fractional frequency reuse," in *Proc. 11th Int. Conf. Des. Reliable Commun. Netw. (DRCN)*, Mar. 2015, pp. 247–250.

[57] H. A. Mustafa, M. Z. Shakir, M. A. Imran, and R. Tafazolli, "Spatial and social paradigms for interference and coverage analysis in underlay D2D network," *IEEE Trans. Veh. Technol.*, vol. 66, no. 10, pp. 9328–9337, Oct. 2017.
[58] M. Xie, X. Jia, M. Zhou, and L. Yang, "Study on energy efficiency of D2D underlay massive MIMO networks with power beacons," in *Proc. 8th Int. Conf. Wireless Commun. Signal Process. (WCSP)*, Oct. 2016, pp. 1–5.
[59] V. Kaur and S. Thangjam, "A stochastic geometry analysis of RF energy harvesting based D2D communication in downlink cellular networks," in *Proc. 1st Int. Conf. Inf. Process. (IICIP)*, Aug. 2016, pp. 1–5.
[60] H. A. Mustafa, M. Z. Shakir, M. A. Imran, A. Imran, and R. Tafazolli, "Coverage gain and device-to-device user density: Stochastic geometry modeling and analysis," *IEEE Commun. Lett.*, vol. 19, no. 10, pp. 1742–1745, Oct. 2015.
[61] Z. Zhang, R. Q. Hu, and Y. Qian, "D2D communication underlay in uplink cellular networks with distance based power control," in *Proc. IEEE Int. Conf. Commun. (ICC)*, May 2016, pp. 1–6.
[62] Z. Liu, T. Peng, H. Chen, and W. Wang, "Optimal D2D user allocation over multi-bands under heterogeneous networks," in *Proc. IEEE Global Commun. Conf. (GLOBECOM)*, Dec. 2012, pp. 1339–1344.
[63] S. Badri, M. Naslcheraghi, and M. Rasti, "Performance analysis of joint pairing and mode selection in D2D communications with FD radios," in *Proc. IEEE Wireless Commun. Netw. Conf. (WCNC)*, Apr. 2018, pp. 1–6.
[64] I. Atzeni and M. Kountouris. (2016). "Performance analysis of partial interference cancellation in multi-antenna UDNs." [Online]. Available: https://arxiv.org/abs/1611.05002
[65] Y. Zhong, X. Ge, H. H. Yang, T. Han, and Q. Li, "Traffic matching in 5G ultra-dense networks," *IEEE Commun. Mag.*, vol. 56, no. 8, pp. 100–105, Aug. 2018.
[66] Y. Zhong, X. Ge, T. Han, Q. Li, and J. Zhang, "Tradeoff between delay and physical layer security in wireless networks," *IEEE J. Sel. Areas Commun.*, vol. 36, no. 7, pp. 1635–1647, Jul. 2018.
[67] A. Azari and C. Cavdar. (2018). "Performance evaluation and optimization of LPWA IoT networks: A stochastic geometry approach." [Online]. Available: https://arxiv.org/abs/1807.06463
[68] M. Haenggi, *Stochastic Geometry for Wireless Networks*. Cambridge, U.K.: Cambridge Univ. Press, 2012.
[69] F. Baccelli and S. Zuyev, "Stochastic geometry models of mobile communication networks," *Frontiers Queueing*, vol. 5, pp. 227–243, Jan. 1997.
[70] R. Vaze, K. T. Truong, S. Weber, and R. W. Heath, "Two-way transmission capacity of wireless ad-hoc networks," *IEEE Trans. Wireless Commun.*, vol. 10, no. 6, pp. 1966–1975, Jun. 2011.
[71] C. M. Fortuin, P. W. Kasteleyn, and J. Ginibre, "Correlation inequalities on some partially ordered sets," *Commun. Math. Phys.*, vol. 22, no. 2, pp. 89–103, Jun. 1971.
[72] I. Atzeni and M. Kountouris, "Full-duplex MIMO small-cell networks with interference cancellation," *IEEE Trans. Wireless Commun.*, vol. 16, no. 12, pp. 8362–8376, Dec. 2017.
[73] N. Jindal, J. G. Andrews, and S. Weber, "Rethinking MIMO for wireless networks: Linear throughput increases with multiple receive antennas," in *Proc. IEEE Int. Conf. Commun.*, Jun. 2008, pp. 1–6.
[74] Z. Gao, L. Dai, D. Mi, Z. Wang, M. A. Imran, and M. Z. Shakir, "MmWave massive-MIMO-based wireless backhaul for the 5G ultra-dense network," *IEEE Wireless Commun.*, vol. 22, no. 5, pp. 13–21, Oct. 2015.
[75] V. Lucarini, "Symmetry-break in Voronoi tessellations," *Symmetry*, vol. 1, no. 1, pp. 21–54, 2009.
[76] A. A. Abouda and S. Häggman, "Effect of mutual coupling on capacity of MIMO wireless channels in high SNR scenario," *Prog. Electromagn. Res.*, vol. 65, pp. 27–40, Jun. 2006.
[77] L. Lovasz, "On the Shannon capacity of a graph," *IEEE Trans. Inf. Theory*, vol. 25, no. 1, pp. 1–7, Jan. 1979.
[78] A. Chan and K. Li. "Wireless communication systems." U.S. Patent 11 113 266, Apr. 20, 2006. [Online]. Available: https://patents.google.com/patent/US20060084504A1/en
[79] P. P. Dyke, *An Introduction to Laplace Transforms and Fourier Series*. London, U.K.: Springer, 2014. [Online]. Available: https://link.springer.com/book/10.1007%2F978-1-4471-6395-4. doi: 10.1007/978-1-4471-6395-4.
[80] Z. Tong and M. Haenggi, "Throughput analysis for full-duplex wireless networks with imperfect self-interference cancellation," *IEEE Trans. Commun.*, vol. 63, no. 11, pp. 4490–4500, Nov. 2015.

FAIZAN QAMAR received the B.E. degree in electronics from Hamdard University, Karachi, Pakistan, in 2010, and the M.E. degree in telecommunication from NED University, Karachi, in 2013. He is currently pursuing the Ph.D. degree in electrical engineering (major in wireless communication) with the Faculty of Engineering, University of Malaya, Kuala Lumpur, Malaysia. He has more than seven years of research and teaching experience. He has authored or coauthored a number of ISI journals and IEEE conference papers. His research interests include wireless networks, interference management, and millimeter-wave communication for 5G.

KAHARUDIN DIMYATI received the B.E. degree in electrical from the University of Malaya, in 1992, and the Ph.D. degree in communication systems from the University of Wales Swansea, U.K., in 1996. He is currently a Professor with the Department of Electrical Engineering, University of Malaya, Kuala Lumpur, Malaysia. He has supervised to the completion, to date, of 15 Ph.D. and 33 masters' research students. He has published more than 100 papers in reputed journals. His research interests include wireless communication, optical communication, and coding theory. He is a member of IET, U.K., IEICE, Japan, and IEM, Malaysia. He is also a Professional Engineer in Malaysia and a Chartered Engineer in U.K.

MHD NOUR HINDIA received the Ph.D. degree from the Faculty of Engineering in Telecommunication, University of Malaya, in 2015. He is working in the field of wireless communications, especially in channel sounding, network planning, converge estimation, handover, scheduling, and quality-of-service enhancement for 5G Networks. He is also working with Research Group in Modulation and Coding Scheme for the Internet of Thing for Future Networks. He has authored or coauthored a number of Science Citation Index (SCI) journals and conference papers. He has also participated as a Reviewer and a Committee Member of a number of ISI journals and conferences.

KAMARUL ARIFFIN NOORDIN received the B.Eng. (Hons.) and M.Eng.Sc. degrees from the University of Malaya, Kuala Lumpur, Malaysia, in 1998 and 2001 respectively, and the Ph.D. degree in communication systems from Lancaster University, U.K., in 2009. He is currently an Associate Professor with the Department of Electrical Engineering, University of Malaya. His research interests include resource allocation in wireless networks, cognitive radio networks, device-to-device communications, network modeling, and performance analysis.

IRAJ SADEGH AMIRI received the B.Sc. degree in applied physics from the Public University of Oroumiyeh, Iran, in 2001, the M.Sc. degree (Hons.) from Universiti Teknologi Malaysia (UTM), in 2009, and the Ph.D. degree in photonics, in 2014. He has published over 100 ISI journal papers and 250 research papers, including Scopus papers, conference papers, books/chapters, and international journal papers in optical soliton communications, laser physics, photonics, fiber optics, nonlinear optics, quantum cryptography, and nanotechnology engineering.